

Iterative thermodynamic modelling—Part 2: Tracing equilibrium relationships between minerals in metamorphic rocks

Pierre Lanari  | Jörg Hermann 

Institute of Geological Sciences, University of Bern, Bern, Switzerland

Correspondence

Pierre Lanari, Institute of Geological Sciences, University of Bern, Baltzstrasse 1+3, 3012 Bern, Switzerland.
Email: pierre.lanari@geo.unibe.ch

Handling Editor: Katy Evans

Abstract

Understanding equilibrium relationships between minerals is a fundamental goal of metamorphic petrology, especially for the quantification of metamorphic conditions recorded by crustal rocks. Information on pressure (P) and temperature (T) can be derived from mineral compositions based on the a priori assumption that frozen-in assemblages reflect chemical equilibrium at the time of formation. While the stable coexistence of minerals is commonly assessed from a combination of microstructural criteria and interpretation of phase diagrams, there is no robust modelling strategy available so far for the unambiguous recognition of minerals that grew at different conditions. This study uses iterative thermodynamic models and the computer program BINGO-ANTIDOTE to propose a general strategy for assessing the stable coexistence of minerals and therefore for tracing multiple partial equilibrium relationships preserved in metapelites to reconstruct their P – T evolutions. First the principles of this approach are elaborated in a theoretical example. Application to a metapelite from the Western Central Alps reveals a detailed, clockwise P – T path with at least four different equilibration stages including a poorly defined peak pressure at 1–1.1 GPa, ~560°C, followed by peak temperatures of ~620°C at 0.9 GPa and a late amphibolite stage at ~580°C, 0.65 GPa. The investigation of the natural metapelite via iterative thermodynamic models (ITM) allows the observed mineral formation sequence to be combined with a higher accuracy with variable mineral compositions and results in a detailed P – T path. The metastable perseverance of one or more mineral phases can be statistically inferred via ITM. In the investigated metapelite, only ~50 vol.% of the rock volume equilibrated at peak temperature conditions of 620°C. In addition, ITM enables a more detailed investigation of partial re-equilibration by diffusion during subsequent metamorphic stages, showing that prograde garnet growth could have been modified during subsequent 10 Ma of amphibolite facies metamorphism in the Central Alps.

KEYWORDS

BINGO-ANTIDOTE, local bulk composition, metamorphism, metapelite, thermodynamics

1 | INTRODUCTION

Although the assumption of equilibrium has led to great strides in our understanding of metamorphism and tectonics in recent years, finding petrological and microstructural criteria for assessing the stable coexistence of minerals remains a long-standing problem in metamorphic petrology and petrochronology. The assumption that minerals of an assemblage represent a fossil equilibrium state in a rock can lead to errors and misinterpretation of pressure–temperature (P – T) conditions obtained via thermobarometric calculations and of crystallization ages (Engi, Lanari, & Kohn 2017). The majority of techniques for thermobarometry require assumptions of chemical equilibrium relationships such as the determination of the *inferred peak assemblage* or *co-existing phases*. But none of the techniques based on equilibrium thermodynamics provide a robust way to validate these assumptions. There is a common observation in metamorphic rocks of zoned minerals (plagioclase, phengite, garnet) occurring in multiple structural and textural positions. This inability of the rocks to fully equilibrate reflects the importance of kinetic processes, which are able to keep pace with changes in pressure and temperature conditions. Most of metamorphic rocks therefore preserve a mosaic of local equilibria (Korzhinskii, 1959; Loomis, 1979; Powell, 1978; Thompson, 1955) documenting multiple stages of their travel through the interior of the Earth. This opportunity, however, poses also the biggest problem in decoding the ‘flight recorder’ of minerals and their compositions, as a rock wide equilibrium clearly has not been achieved. There have been several approaches to overcome these limitations.

Inverse thermodynamic models aim to retrieve equilibrium conditions from local phase compositions of an assemblage of minerals (Berman, 1991; Powell & Holland, 1988, 1994; Vidal & Parra, 2000). The convergence of reactions in the P – T space indicates that the selected mineral compositions are consistent with chemical equilibrium. What it does not provide, in the absence of Gibbs energy minimization (GEM), is the unequivocal evidence that the considered phases were in chemical equilibrium for the reactive bulk composition and the expected abundance of phases (Lanari & Duesterhoeft, 2019). In other words, not all the phases used to calculate the P – T conditions in an inverse model might be stable for an appropriate bulk composition at the given P – T conditions. Support from compositional maps can assist the interpretations by providing detailed microstructural information (Di Rosa, De Giorgi, Marroni, & Vidal 2017; Lanari et al., 2012, 2013; Scheffer et al., 2016; Vidal et al., 2006), but P – T estimates obtained via an inverse model strongly rely on a priori assumptions of equilibrium relationships.

An alternative strategy is to use forward thermodynamic models such as isochemical P – T phase diagrams combined

Highlights

- Application of iterative thermodynamic models to metapelite.
- Identification of prograde, peak and retrograde minerals.
- Post-growth diffusion can affect garnet thermobarometry.
- Partial re-equilibration during peak metamorphism.

with isopleth thermobarometry (Powell & Holland, 2008). These tools are commonly used to depict the evolution of the stable mineral assemblage, modes and compositions for a given bulk system composition (De Capitani & Petrakakis, 2010; Hensen, 1971; White, Powell, & Baldwin 2008; Yakymchuk, 2017). The numerical strategy reflects the tendency of any rock system to minimize its total Gibbs energy and to converge towards a global state of thermodynamic equilibrium. Several numerical techniques have been developed to reproduce this behaviour (Brown & Skinner, 1974; Connolly & Kerrick, 1987; de Capitani & Brown, 1987; Powell & Holland, 1994; Spear, 1988b), some of them relying on GEM in a system at fixed P and T , and for a given bulk rock composition (X_{bulk}). However, the preservation of metastable mineral relics and compositional zoning in natural rocks, for example during prograde metamorphism, can significantly affect the simulations made for peak conditions, increasing the risk of error and misinterpretations (Evans, 2004; Indares, White & Powell 2008; Lanari & Duesterhoeft, 2019; Lanari & Engi, 2017; Marmo, Clarke, & Powell 2002; Spear, 1988a). Only rarely, all the information (phase stability, phase composition and phase abundance) is coherently used in this approach (Ceccato, Goncalves, & Pennacchioni 2020; Guevara & Caddick, 2016).

A third strategy is to apply iterative thermodynamic models (ITM) integrated with quantitative compositional mapping (Lanari & Duesterhoeft, 2019). This hybrid approach relies on the determination of local bulk compositions (LBC), each of them measured from a given region of interest in the sample, while excluding unreactive phases. The LBC is then assumed to approximate the reactive (or effective) bulk composition of a given stage. One of the key features is the correspondence between the LBC and the direct observations (assemblage, mineral modes and compositions) in the same volume (Lanari & Engi, 2017). This mutual correspondence permits to build a fully quantitative comparison between model and observations as well as providing a statistical framework for evaluating model quality. This approach was implemented in the software solution BINGO-ANTIDOTE,

which is described in the companion paper (Dueterhoeft & Lanari, 2020). Two fundamental questions remain: (a) how do mineralogical variations at the thin-section scale affect (or not) the result of ITMs? (b) Can we successfully track multiple partial equilibrations in order to obtain P – T paths from complex metamorphic rocks? These questions are investigated in the following by combining both theoretical and natural application examples. The results provide guidelines and a general strategy on how to identify disequilibrium features—characteristic of most metamorphic rocks—and to quantify their potential effects on thermodynamic calculations made at equilibrium.

2 | THEORETICAL EXAMPLE

The application of ITM for assessing equilibrium relationships is first tested by combining P – T isochemical phase diagrams and Monte Carlo simulations for a theoretical case study. A *virtual metapelite* having a bulk rock composition taken from Yakymchuk et al. (2017) was selected. The rock is first assumed to have been fully equilibrated at 650°C and 0.8 GPa and then fully preserved from retrogression upon cooling and exhumation. Thermodynamic computations were performed using the internally consistent data set of Holland and Powell (2011), the activity models of White et al. (2014) and the Gibbs energy minimizer THERIAK (de Capitani & Brown, 1987; De Capitani & Petrakakis, 2010). The P – T isochemical phase diagram computed for the bulk rock composition via GEM is presented in Figure 1a. The reference mineral assemblage, mineral modes (vol.%) and compositions (atom per formula unit, apfu) corresponding to the ‘observations’ were set using the model output at 650°C and 0.8 GPa (red spot in Figure 1a). At these conditions, the observations must be perfectly reproduced by the model. The mineral assemblage predicted to be stable is garnet (4.3 vol.%), muscovite (19.8%), biotite (21.3%), staurolite (5.4%), plagioclase (20.1%), ilmenite (1.1%) and quartz (28.0%). Diagnostic mineral compositions are reported in Table 1. Mineral abbreviations are from Whitney and Evans (2010).

2.1 | Model [1]—equilibrium | bulk rock composition | variable P – T

The goal of *Model [1]* is to illustrate a simple application of ITM. The bulk rock composition and reference data (mineral assemblage, modes and compositions) defined above were used as input in BINGO-ANTIDOTE. Note that this is not possible for natural samples. The mineral modes corresponding to the bulk rock composition are generally unknown because modes are heterogeneous across the rock

volume (Dueterhoeft & Lanari, 2020). Nevertheless, maps of the model-quality factors Q_{asm} , Q_{vol} and Q_{cmp} that quantify how the model reproduces the observed mineral assemblage, modes and mineral compositions as well as a map of a global evaluation criterion Q_{total} were generated using *Recipe #2* of ANTIDOTE (*P – T map of Q factors*) for a P – T range of 500–650°C and 0.4–1 GPa; results are shown in Figure 1. The formalism used by BINGO to calculate the model-quality factors Q_{asm} , Q_{vol} , Q_{cmp} and Q_{total} is given in Dueterhoeft and Lanari (2020). *Recipe #2* of ANTIDOTE is a simple mapping function producing P – T maps of model-quality factors. The map of Q_{asm} mimics the isochemical phase diagram with a maximum of 100% reached in the stability field Grt+St+Pl+Bt+Qz+Ms+Ilm surrounding the reference P – T conditions of 650°C and 0.8 GPa. By contrast, the model-quality factors corresponding to the mineral modes Q_{vol} and to the mineral compositions Q_{cmp} have little apparent relationships with the geometry of the stability fields. This behaviour is normal as only the matching phases are used in the evaluation of Q_{vol} and Q_{cmp} (see discussion in Dueterhoeft & Lanari, 2020). Both functions exhibit smoother gradients with global maxima of 100% at the reference conditions. This reflects multi-variant equilibria that are responsible for a gradual change in mineral composition and abundance. The map of Q_{total} is shown in Figure 1e with a maximum of 100% at the reference conditions. At these conditions, the modelled and ‘observed’ mineral assemblages modes and compositions are identical. This first example shows that for a well-equilibrated sample, no retrogression and perfect thermodynamic data, the inversion performed using *Recipe #1* of ANTIDOTE (*Find optimal P – T (-X)*) would converge to the ‘optimal’ P – T conditions, in this case corresponding to the equilibrium conditions of the peak mineral assemblage. The example also shows how important the mineral mode and compositional isopleths are for defining P – T compositions within the assumed field of the peak assemblage (see also Powell & Holland, 2008).

2.2 | Model [2a]—equilibrium | LBC | fixed P – T

The goal of *Model [2a]* is to simulate the investigation of the same virtual metapelite but this time using LBC instead of the bulk rock composition. The interest of this second model is to simulate the use of LBC as this can be easily obtained from compositional maps for any given area-of-interest (Lanari et al., 2019). The reference mineral assemblage and mineral compositions are also defined based on the model outcomes at 650°C and 0.8 GPa, but the phase proportions can change in every simulation. This reflects possible changes in mineral modes within a given

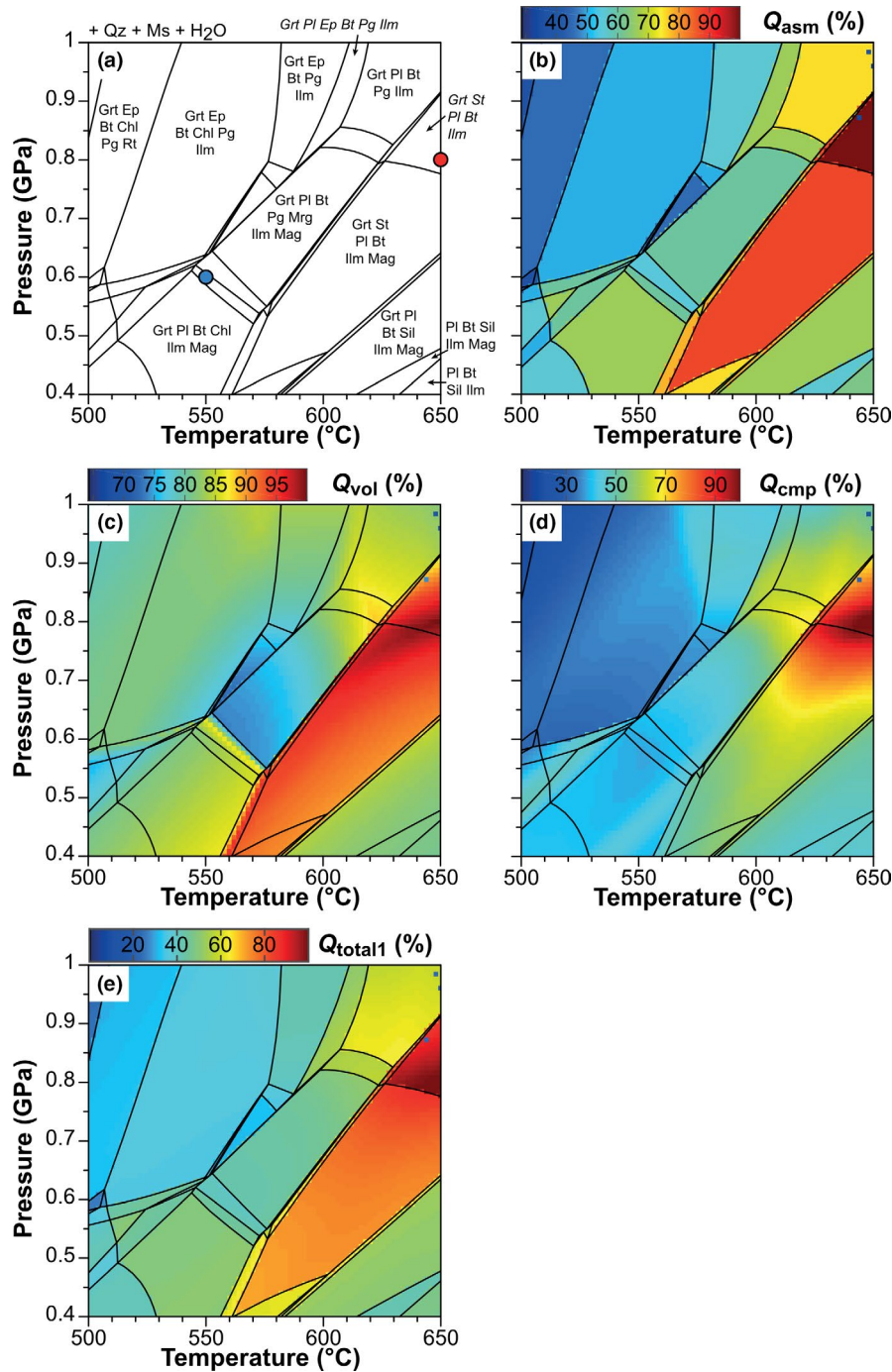


FIGURE 1 Results of Iterative thermodynamic models (ITM) for a virtual metapelite (see text for details). (a) P - T equilibrium phase diagram. The red spot shows the conditions of 650°C and 0.8 GPa at which the rock is assumed to have been fully re-equilibrated. (b) Map of quality factor for the assemblage Q_{asm} and stability fields taken from the phase diagram shown in (a). (c) Map of quality factor for the mineral modes Q_{vol} . (d) Map of quality factor for the mineral compositions Q_{cmp} . (e) Map of quality factor for Q_{total1} . Mineral abbreviations in this and the following figures are from Whitney and Evans (2010)

area-of-interest while keeping the mineral assemblage and compositions fixed. Random molar abundances assuming a uniform distribution on the interval $[n_i - 0.75 \times n_p, n_i + 0.75 \times n_p]$ were used to generate 10,000 pseudo-LBC. The corresponding volume fractions range from 0.85 vol.% (iteration #4525, see Table 1) to 12.53% (#6358) for garnet, from 4.86% (#4033) to 43.82% (#4615) for biotite, from 4.50% (#1223) to 43.20% (#7134) for plagioclase, from 1.07% (#9706) to 15.02% (#2005) for staurolite and from 0.33% (#4033) to 3.10% (#7811) for ilmenite. This distribution simulates the possible choice of different domains within a thin section, resulting in variable mineral

proportions and thus variable LBC. In this situation—assuming equilibrium, a fixed assemblage and fixed P - T conditions—the predicted mineral assemblages and mineral compositions do not vary for the different simulations at the peak conditions (Table 1). The modelled mineral modes are matching the input and the values of Q_{asm} , Q_{vol} , Q_{cmp} and Q_{total1} are systematically 100%. Minimization of $-Q_{total1}$ using *Recipe #1* of ANTIDOTE (*Find optimal P - T (-X)*) would converge to the same optimal P - T conditions of 650°C and 0.8 GPa whatever the phase proportions in the considered domain are. This result demonstrates that *in an equilibrium scenario, the investigation of any spatial*

TABLE 1 Input and selected outputs of Model [2a]. Mineral abbreviations are from Whitney and Evans (2010)

Simulation	Input of GEM													Output of GEM														
	Mineral modes for LEB (vol.%)													Plagioclase			Garnet			Muscovite			Biotite			Staurolite		
	Pl	Grt	Ms	Bt	St	Ilm	Qz	X _{ab}	X _{an}	X _{alm}	X _{prp}	X _{grs}	X _{sps}	Si (apfu)	X _{Mg}	Si	X _{Mg}	Si (apfu)	X _{Mg}	Si	X _{Mg}							
Bulk	20.08	4.30	19.83	21.30	5.40	1.12	27.97	0.710	0.281	0.684	0.177	0.088	0.052	3.040	0.495	2.630	0.520	0.292										
17	11.35	7.97	33.34	11.34	5.13	0.70	30.16	0.710	0.281	0.684	0.177	0.088	0.052	3.040	0.495	2.630	0.520	0.292										
555	11.31	8.04	18.07	16.12	11.07	0.79	34.61	0.710	0.281	0.684	0.177	0.088	0.052	3.040	0.495	2.630	0.520	0.292										
787	32.21	4.33	7.68	22.63	2.62	1.60	28.92	0.710	0.281	0.684	0.177	0.088	0.052	3.040	0.495	2.630	0.520	0.292										
850	26.63	5.76	6.86	15.61	6.23	1.26	37.64	0.710	0.281	0.684	0.177	0.088	0.052	3.040	0.495	2.630	0.520	0.292										
1079	8.08	5.39	28.89	8.20	11.42	2.12	35.91	0.710	0.281	0.684	0.177	0.088	0.052	3.040	0.495	2.630	0.520	0.292										
1223	4.50	6.08	30.28	28.37	4.85	1.13	24.80	0.710	0.281	0.684	0.177	0.088	0.052	3.040	0.495	2.630	0.520	0.292										
1642	25.61	2.94	19.90	20.42	4.77	1.00	25.35	0.710	0.281	0.684	0.177	0.088	0.052	3.040	0.495	2.630	0.520	0.292										
1832	22.83	4.88	22.82	24.63	5.39	0.44	19.01	0.710	0.281	0.684	0.177	0.088	0.052	3.040	0.495	2.630	0.520	0.292										
1940	25.31	4.64	16.02	27.00	4.12	1.39	21.51	0.710	0.281	0.684	0.177	0.088	0.052	3.040	0.495	2.630	0.520	0.292										
2005	10.96	2.29	9.52	14.49	15.02	2.85	44.88	0.710	0.281	0.684	0.177	0.088	0.052	3.040	0.495	2.630	0.520	0.292										
2236	26.00	6.89	9.07	7.42	11.97	1.59	37.06	0.710	0.281	0.684	0.177	0.088	0.052	3.040	0.495	2.630	0.520	0.292										
2922	12.86	5.19	16.67	10.28	2.71	2.83	49.48	0.710	0.281	0.684	0.177	0.088	0.052	3.040	0.495	2.630	0.520	0.292										
3180	12.90	1.44	16.07	34.88	2.71	0.74	31.26	0.710	0.281	0.684	0.177	0.088	0.052	3.040	0.495	2.630	0.520	0.292										
3720	9.82	2.11	25.71	29.06	6.04	1.24	26.02	0.710	0.281	0.684	0.177	0.088	0.052	3.040	0.495	2.630	0.520	0.292										
4033	30.02	4.73	27.03	4.86	8.32	0.33	24.71	0.710	0.281	0.684	0.177	0.088	0.052	3.040	0.495	2.630	0.520	0.292										
4525	25.75	0.85	22.44	22.72	6.46	0.54	21.24	0.710	0.281	0.684	0.177	0.088	0.052	3.040	0.495	2.630	0.520	0.292										
4615	7.77	1.29	10.40	43.82	1.91	1.69	33.13	0.710	0.281	0.684	0.177	0.088	0.052	3.040	0.495	2.630	0.520	0.292										
4798	23.08	3.09	12.77	26.40	5.79	0.66	28.23	0.710	0.281	0.684	0.177	0.088	0.052	3.040	0.495	2.630	0.520	0.292										
5326	28.38	5.59	4.36	30.03	7.48	0.87	23.29	0.710	0.281	0.684	0.177	0.088	0.052	3.040	0.495	2.630	0.520	0.292										
6358	8.51	12.53	8.57	12.85	8.88	1.40	47.24	0.710	0.281	0.684	0.177	0.088	0.052	3.040	0.495	2.630	0.520	0.292										
6489	22.33	1.82	24.76	23.37	1.33	0.37	26.03	0.710	0.281	0.684	0.177	0.088	0.052	3.040	0.495	2.630	0.520	0.292										
7134	43.20	1.35	6.33	9.93	3.12	1.09	34.97	0.710	0.281	0.684	0.177	0.088	0.052	3.040	0.495	2.630	0.520	0.292										
7811	12.85	11.36	8.18	12.95	6.51	3.10	45.05	0.710	0.281	0.684	0.177	0.088	0.052	3.040	0.495	2.630	0.520	0.292										
7927	18.94	3.83	22.98	25.52	5.84	1.00	21.88	0.710	0.281	0.684	0.177	0.088	0.052	3.040	0.495	2.630	0.520	0.292										
8473	13.38	5.47	30.27	16.51	8.30	0.91	25.17	0.710	0.281	0.684	0.177	0.088	0.052	3.040	0.495	2.630	0.520	0.292										
8678	6.78	2.27	43.60	8.13	3.58	0.42	35.23	0.710	0.281	0.684	0.177	0.088	0.052	3.040	0.495	2.630	0.520	0.292										
9706	17.44	5.03	25.51	28.55	1.07	0.65	21.75	0.710	0.281	0.684	0.177	0.088	0.052	3.040	0.495	2.630	0.520	0.292										
9708	20.89	5.21	20.27	25.24	2.83	1.45	24.11	0.710	0.281	0.684	0.177	0.088	0.052	3.040	0.495	2.630	0.520	0.292										
9977	25.52	3.00	19.26	24.50	2.85	0.85	24.01	0.710	0.281	0.684	0.177	0.088	0.052	3.040	0.495	2.630	0.520	0.292										

domain of a metamorphic rock with its own LBC results in identical modelled mineral assemblages and mineral compositions but with different mineral modes at the P – T conditions of equilibrium.

2.3 | Model [2b]—equilibrium | LBC | variable P – T

The bulk rock scenario of *Model [1]* was selected together with three simulations from *Model [2a]* and the corresponding mineral modes shown in Figure 2. Simulation #6358 reflects a Grt rich domain (Figure 2b), #7134 a Pl+Qz rich domain (Figure 2c) and #8678 a Pl+Ms rich domain (Figure 2c). Such heterogeneities are commonly observed in natural metapelites as illustrated below in the second application example. *Model [2b]* consists for each bulk composition of an isochemical phase diagram combined with a quality-factor map of Q_{total} ; results are shown in Figure 3. At least two important conclusions can be drawn from this simulation. Firstly, the optimal value of Q_{total} of 100% is systematically found at the reference conditions (as already demonstrated in *Model [2a]*) and therefore the search routine implemented in *Recipe #2* of ANTIDOTE would converge to the optimal P – T conditions for each case. However, the geometry of the isochemical phase diagrams changes significantly (Figure 3). Garnet for example is predicted to be stable for the entire P – T range in the phase diagram shown in Figure 3b corresponding to the garnet-rich LBC (Figure 2b), and has a much restricted range of stability in the phase diagram of Figure 3c corresponding to a garnet-poor domain (Figure 2c). Such behaviour is normal as the positions of many reactions are controlled by the bulk composition as also simulated by Palin, Weller, Waters, and Dyck (2016). However, contrary to what these authors concluded, it does not affect the absolute P – T conditions of equilibrium as demonstrated above for a well-equilibrated mineral assemblage (see *Model [2a]* and Table 1). By contrast, deviations are only expected for partially re-equilibrated rocks (Lanari & Duisterhoeft, 2019; Lanari & Engi, 2017); this scenario is further investigated in the following simulation.

2.4 | Model [3]—local equilibrium (mineral relics) | LBC | fixed P – T

The goal of *Model [3]* is to simulate the investigation of the same virtual metapelite using LBC but, in this case, the rock is assumed to have only partially been re-equilibrated at the peak conditions of 650°C and 0.8 GPa. Plagioclase is arbitrarily assumed in *Model [3]* to have formed at 550°C and 0.6 GPa, during prograde metamorphism, near the plagioclase in curve and it has been prevented to re-equilibrate by diffusion or net transfer reaction later on. The composition of the metastable plagioclase—modelled at 550°C and 0.6 GPa—is $\text{Ab}_{0.64}\text{An}_{0.36}\text{San}_{0.00}$, which moderately diverges from the composition previously predicted to be stable at the peak conditions ($\text{Ab}_{0.71}\text{An}_{0.28}\text{San}_{0.01}$ at 650°C and 0.8 GPa). Random molar abundances assuming uniform distributions on the interval $[n_i - 0.75 \times n_i, n_i + 0.75 \times n_i]$ were used to generate 10,000 pseudo-LBC using the compositions of the stable garnet, staurolite, biotite, quartz, muscovite, ilmenite and metastable plagioclase. In this simulation, the values of Q_{total} vary and never reach the optimal value of 100%, which indicates that the simulation fails to reproduce the reference mineral compositions and modes. By contrast, Q_{asm} is systematically 100% erroneously suggesting that plagioclase was in equilibrium with the other minerals at the peak conditions. The results of *Model [3]* are presented in Figure 4 as Q_{cmp} data of plagioclase, garnet and staurolite relative to the volume fraction of garnet and plagioclase in the corresponding LBC and in Figure 5 as Q_{cmp} (total) relative to four components in the corresponding LBC. An interesting result of *Model [3]* is that the model quality evolves with the fraction of plagioclase used to determine each pseudo-LBC. If more plagioclase is involved, it results in lower model qualities ($Q_{\text{cmp}}^{\text{Pl}} \approx 45\%$ for 40 vol.% of plagioclase), whereas lower plagioclase fractions lead to higher model quality ($Q_{\text{cmp}}^{\text{Pl}} \approx 80\%$ for ~5 vol.% of plagioclase). This effect is propagated towards garnet because of Ca partitioning between garnet and plagioclase and, by repercussion, to staurolite as the Fe–Mg partitioning between garnet and staurolite is affected by the amount of Ca available for garnet. Higher values of $Q_{\text{cmp}}^{\text{Pl}}$ result in higher $Q_{\text{cmp}}^{\text{Grt}}$ and $Q_{\text{cmp}}^{\text{St}}$ (Figure 4).

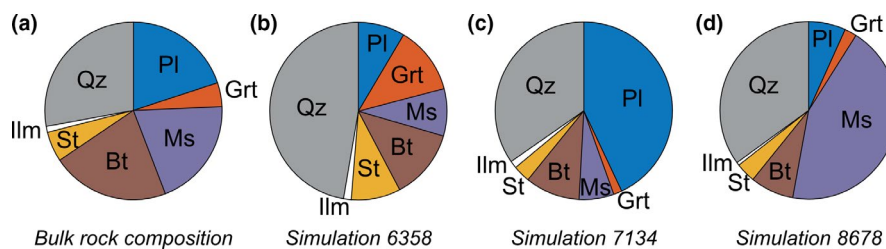


FIGURE 2 Mineral assemblage and mineral modes simulated in *Model [2a]* at 650°C and 0.8 GPa for (a) the bulk rock composition and (b–d) three selected simulations (#6358, #7134 and #8678) corresponding to a garnet-rich, plagioclase-rich and muscovite-rich domains. The quality-factor Q_{total} for each simulation is 100% (see text for details)

FIGURE 3 Simplified P - T phase diagrams combined with quality-factor maps of Q_{total1} for the selection of LBC from *Model [2a]* shown in Figure 2. (a) Bulk rock composition. Local bulk compositions are taken from simulations (b) #6358, (c) #7134 and (d) #7134. Note that the same mineral assemblage is predicted to be stable at 650°C and 0.8 GPa. The garnet-in (abbreviation: Grt in), plagioclase-in (Pl in) and staurolite-in (St in) curves are shown in red, white and black respectively when present

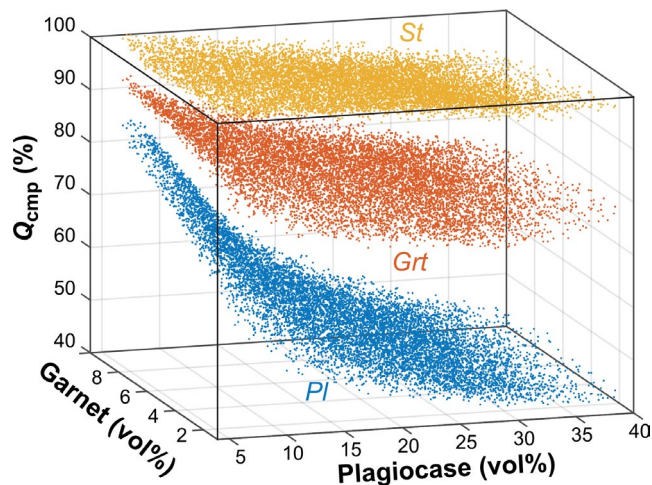
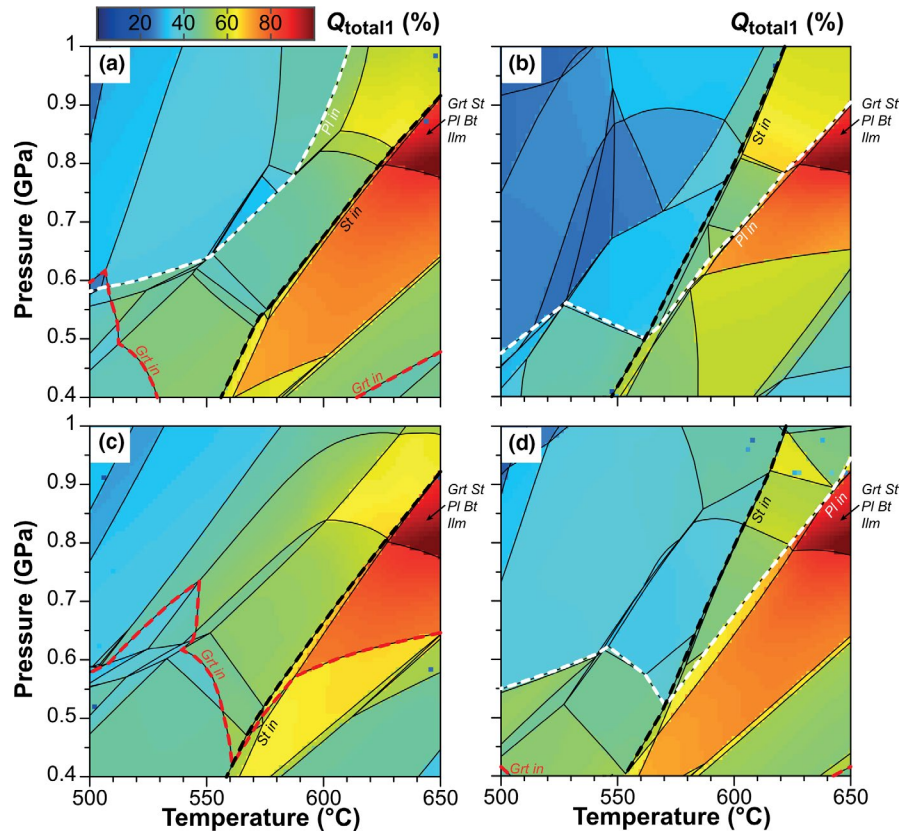


FIGURE 4 Evolution in *Model [3]* of the quality-factor Q_{comp} of plagioclase (blue), garnet (red) and staurolite (yellow) with the fraction of garnet and plagioclase in the LBC (expressed in vol.% of the solid phases)

However, the variations of garnet fractions in LBC do not affect the model quality at fixed plagioclase fractions. Similar effects can be observed between the components of the bulk composition and the quality-factor Q_{comp} (Figure 5). A lower plagioclase fraction in the LBC results in lower Ca and Na contents and in better model quality (up to 96% for 0.75 mol.% of Ca). By contrast, the amount of K (hosted in k-feldspar) and Fe (hosted in garnet, biotite and staurolite) in the LBC does not directly affect the model quality.

This model demonstrates that if a mineral relic—here plagioclase—is not re-equilibrated at the peak condition (a) the modelled assemblage can be misleading and (b) LBC with variable mineral proportions can generate trends in model-quality factors. The selection of an area-of-interest with a low fraction of plagioclase results in higher model quality compared to a domain with a high plagioclase fraction. As plagioclase mode is ~20 vol.% in the virtual metapelite, a model based on the bulk rock composition is expected to have a significant discrepancy at the peak conditions.

2.5 | Interpretations

The following interpretations can be drawn from the four theoretical simulations presented above:

1. For well-equilibrated samples (and perfect thermodynamic data), ITM based on the bulk rock composition or any LBC will converge to the ‘optimal’ P - T conditions reflecting equilibration conditions.
2. Within the stability field of the peak assemblage, isopleths of mineral compositions and mineral abundances are very useful to further constrain P - T conditions as discussed in Powell and Holland (2008).
3. For well-equilibrated samples, LBC far from the bulk rock compositions should not be used to predict the position of

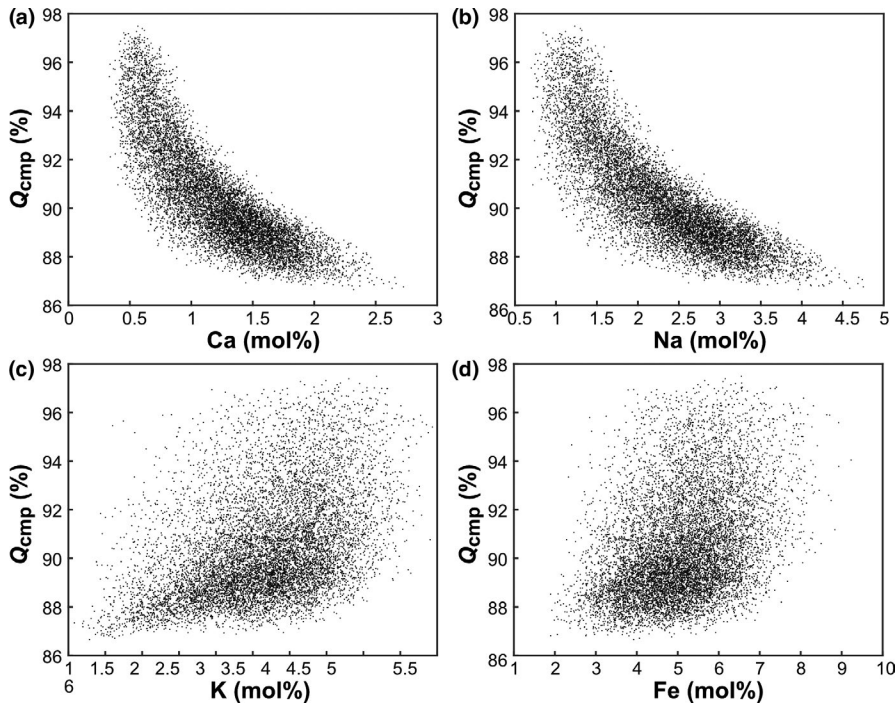


FIGURE 5 Evolution in *Model [3]* of the quality-factor $Q_{\text{cmp}}(\text{total})$ with the molar fraction of (a) Ca, (b) Na, (c) K and (d) Fe (expressed in mol% of the LBC)

mineral reactions in the P – T space far away from the equilibration conditions. The bulk rock composition should be used instead if the purpose is to simulate the possible conditions of mineral forming reactions.

4. For partially equilibrated samples, the fraction of mineral relics used in the LBC estimation can significantly affect the model-quality factors. If mineral relics are present, an area-of-interest containing a lower fraction of them must be favoured instead of the bulk rock composition.
5. For partially re-equilibrated samples, the investigation of the correlation between mineral modes and the model-quality factors can in theory serve to detect the presence of metastable phases that were not fully re-equilibrated at the peak conditions.
6. The modelled mineral assemblage can be ambiguous in case of metastable perseverance and the model-quality factor Q_{cmp} of each solid solution need to be considered in addition to test the assumption of equilibrium.

3 | NATURAL EXAMPLE

A metapelite from Croveo (north of Domodossola) in the Italian Central Alps previously studied by Todd and Engi (1997) and Boston, Rubatto, Hermann, Engi, and Amelin (2017) was reinvestigated. The sample derives from the Mesozoic cover separating the Verampio from the Antigorio nappes in the Western Central Alps. This schist (MA9330) is made of garnet, biotite, white mica, plagioclase, staurolite, kyanite and quartz with the accessory minerals monazite, apatite, rutile, ilmenite and

zircon. The P – T conditions of the metamorphic peak recorded during Alpine barrovian metamorphism were previously determined from the inferred peak assemblage Grt+Bt+Ms+Ilm+Rt+Ky+Qtz (excluding Pl, St and Tur) at $617 \pm 11^\circ\text{C}$ and 0.62 ± 0.05 GPa based on three independent reactions (Todd & Engi, 1997). Rutile thermobarometry indicates lower temperatures around $\sim 565^\circ\text{C}$ ($\text{Zr} = 99 \pm 18$ ppm (15 grains); 1 GPa) and monazite which formed at the expense of allanite above 600°C returned a concordia U–Pb age of 21.7 ± 0.4 Ma (Boston et al., 2017).

3.1 | Compositional mapping

The polished thin section from Boston (2014) was re-analysed using a JEOL JXA-8200 superprobe at the Institute of Geological Sciences of the University of Bern following the analytical procedure described in Lanari and Piccoli (2020). Three areas were investigated via three maps acquired at 15 keV accelerating voltage and a specimen current of 100 nA. Data reduction was performed using XMAPTOOLS 3.2.2 (Lanari et al., 2014, 2019). The X-ray maps were first corrected for time-related drift and surface irregularities using the TOPO map; all the pixels were then classified and calibrated using either the internal standardization procedure including a pseudo-background correction or by manual calibration (Lanari et al., 2019). The analytical conditions are provided in Material S1. Each LBC was generated from density-corrected maps (Lanari & Engi, 2017) assuming an average density of $4,130 \text{ kg/m}^3$ for garnet, $3,090 \text{ kg/m}^3$ for biotite, $2,820 \text{ kg/m}^3$ for muscovite, $2,680 \text{ kg/m}^3$ for

plagioclase, 3,610 kg/m³ for kyanite, 2,620 kg/m³ for quartz, 3,710 kg/m³ for staurolite, 2,650 kg/m³ for chlorite, 4,250 kg/m³ for rutile, 4,720 kg/m³ for ilmenite and 3,150 kg/m³ for apatite. Maps of structural formulas were calculated using the external functions available in the XMAPTOOLS package.

Area 1—Mineral matrix. A rectangular area of 6 × 4.5 mm was investigated using a step size of 6 μm and a dwell time of 100 ms in ~42 hr. The X-ray maps have a resolution of 1,000 × 750 corresponding to a total of 750,000 pixels. The mineral phases biotite (22 internal standards), muscovite (11) and plagioclase (11) were standardized using the internal standardization procedure, whereas quartz, rutile, ilmenite and apatite were standardized using manual calibrations based on theoretical compositions.

Area 2—Garnet–kyanite(±staurolite) assemblage. A rectangular area of 6 × 4.5 mm was investigated using the same step size, dwell time and resolution (6 μm; 100 ms; 1,000 × 750 pixels) in ~42 hr. The mineral phases garnet (15 internal standards) biotite (20), muscovite (8), chlorite (8), kyanite (4), staurolite (3) and plagioclase (3) were standardized using the internal standardization procedure whereas quartz, rutile, ilmenite and apatite were standardized using manual calibrations.

Area 3—Garnet porphyroblast. A squared area of 10 × 10 mm was investigated using a step size of 10 μm and a dwell time of 60 ms in ~34 hr. The X-ray maps have a resolution of 1,000 × 1,000 corresponding to a total of 1,000,000 pixels. The mineral phases garnet (22 internal standards) biotite (5), muscovite (6), staurolite (4) and plagioclase (3)

were standardized using the internal standardization procedure whereas kyanite, quartz, rutile, ilmenite and apatite were standardized using manual calibrations.

The locations of each mapping area on the thin section as well as the mineral maps (mask images) are shown in Figure 6. Representative mineral compositions are given in Table 3 and in Material S2. Maps of end-member fractions of garnet are compiled in Figure 7. Maps of structural formulas are shown in Figure 8 for area 1 and area 2 and in Material S3 for area 3. Temperature maps of biotite using the Ti-in-biotite calibration of Henry, Guidotti, and Thomson (2005) are provided in Material S4.

3.2 | Petrography

The Croveo schist Ma9330 is characterized by synkinematic garnet porphyroblasts that contain relic, oriented quartz ribbons as well as numerous small inclusions of plagioclase, quartz and ilmenite (Figure 6a,b). Allanite occasionally also occurs as inclusion in garnet (Boston et al., 2017). Garnet is surrounded by a foliation marked by kyanite, white mica, plagioclase, biotite and quartz (Figure 6b,d). Kyanite occurs also in grains that are discordant to the foliation (Figure 6d). Accessory rutile is also aligned along the foliation (Figure 6c). Monazite was found exclusively in the mineral matrix (Boston et al., 2017). Staurolite is not aligned along the foliation, partly overgrows kyanite and is

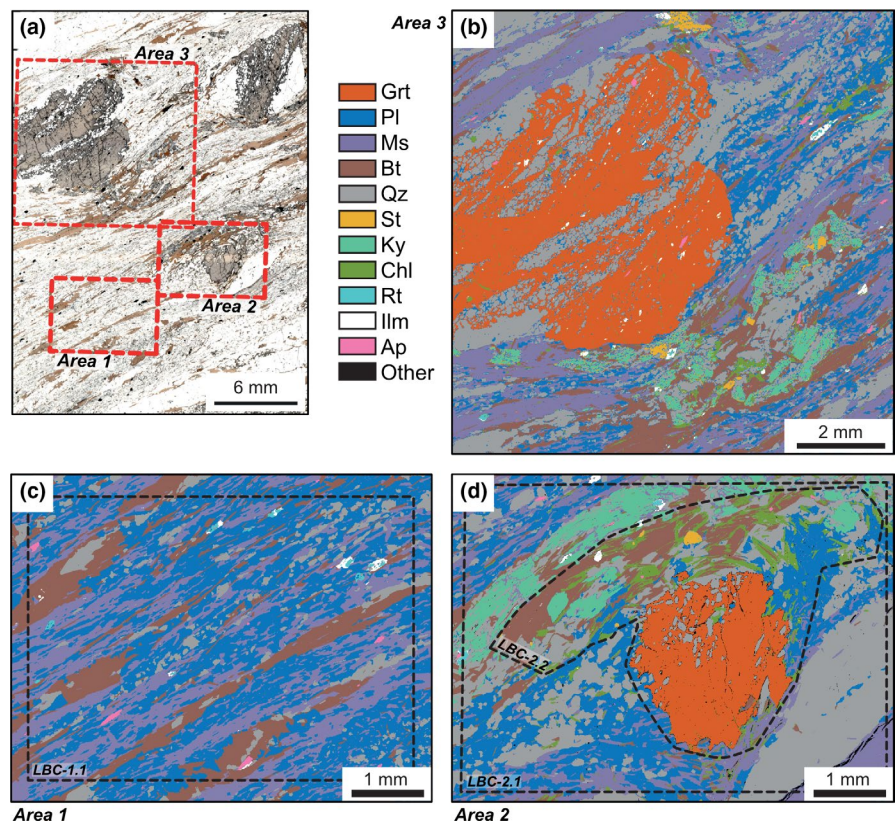


FIGURE 6 Compositional mapping of the sample MA9330 from Todd and Engi (1997) and Boston et al. (2017). (a) Thin-section microphotograph showing the three areas (labelled Area 1, Area 2 and Area 3) used for EPMA X-ray mapping. (b) Mineral map of Area 3 containing a centimetre-size garnet porphyroblast. (c) Mineral map of Area 1, the 'mineral matrix' containing the area-of-interest LBC1.1. (d) Mineral map of Area 2, the 'kyanite domain', containing both area-of-interest LBC2.1 and LBC2.2

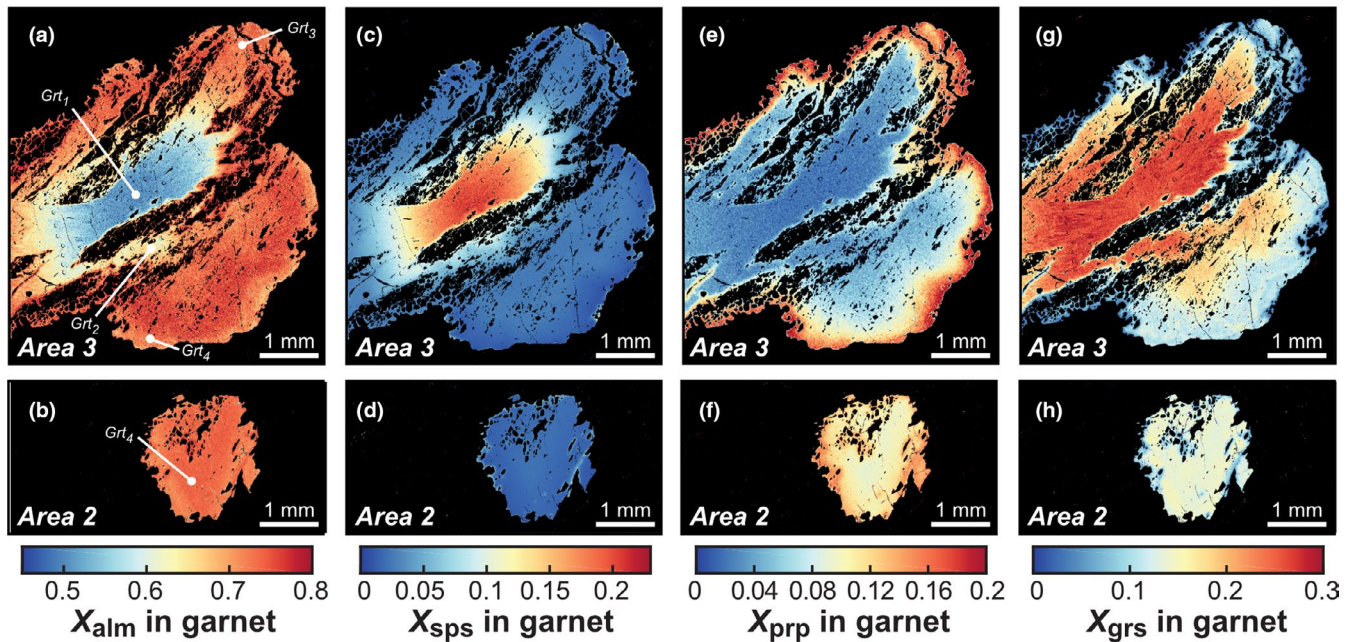


FIGURE 7 Quantitative compositional maps of garnet showing end-member atomic fractions for (a, c, e, g) the porphyroblast in Area 3 and (b, d, f, h) a smaller grain located in Area 2. The colour scale used for each end-member is the same for the two maps

locally in textural equilibrium with chlorite (Figure 6b,d). Retrograde chlorite occurs close to garnet and in biotite-rich domains and is poorly aligned. Ilmenite overgrowths rutile in the mineral matrix (Figure 6c). The mineral matrix in *area 1* (Figure 6a,c) is made of plagioclase (43 vol.%), muscovite (30%), biotite (17%), quartz (9%) and the accessory phases rutile, ilmenite and apatite (<1%). The rock texture is relatively heterogeneous with distinct domains in *area 3* roughly corresponding to each simulation presented in Figure 2. By contrast, the matrix away from the garnet porphyroblasts is more homogeneous.

3.3 | Mineral compositions

Garnet porphyroblasts are compositionally zoned with a bell-shaped decrease in Mn from core ($\text{Alm}_{48}\text{Prp}_4\text{Grs}_{27}\text{Sps}_{19}$) to rim ($\text{Alm}_{75}\text{Prp}_7\text{Grs}_{14}\text{Sps}_2$) associated with an increase in Fe (Figure 7). Both Mg and Ca exhibit different zoning patterns with relatively homogeneous cores, mantles and thin rims (0.5–1 mm in radius) marked by a sharp compositional change (Figure 7e,g). The garnet grain located in area 2 is cut far away from its centre and exhibits only minor compositional variations occurring within the thin rim (Figure 7). Peripheral increase in Mn (near-rim kick-up with X_{sps} locally reaching 0.08–0.10) reflects minor garnet resorption and retrodiffusion (e.g. Kohn & Spear, 2000). Garnet compositional zoning divided into four groups (Grt_1 , Grt_2 , Grt_3 and Grt_4) is first interpreted to reflect changes in growth conditions without significant post-growth compositional modification by intragranular—potential biases

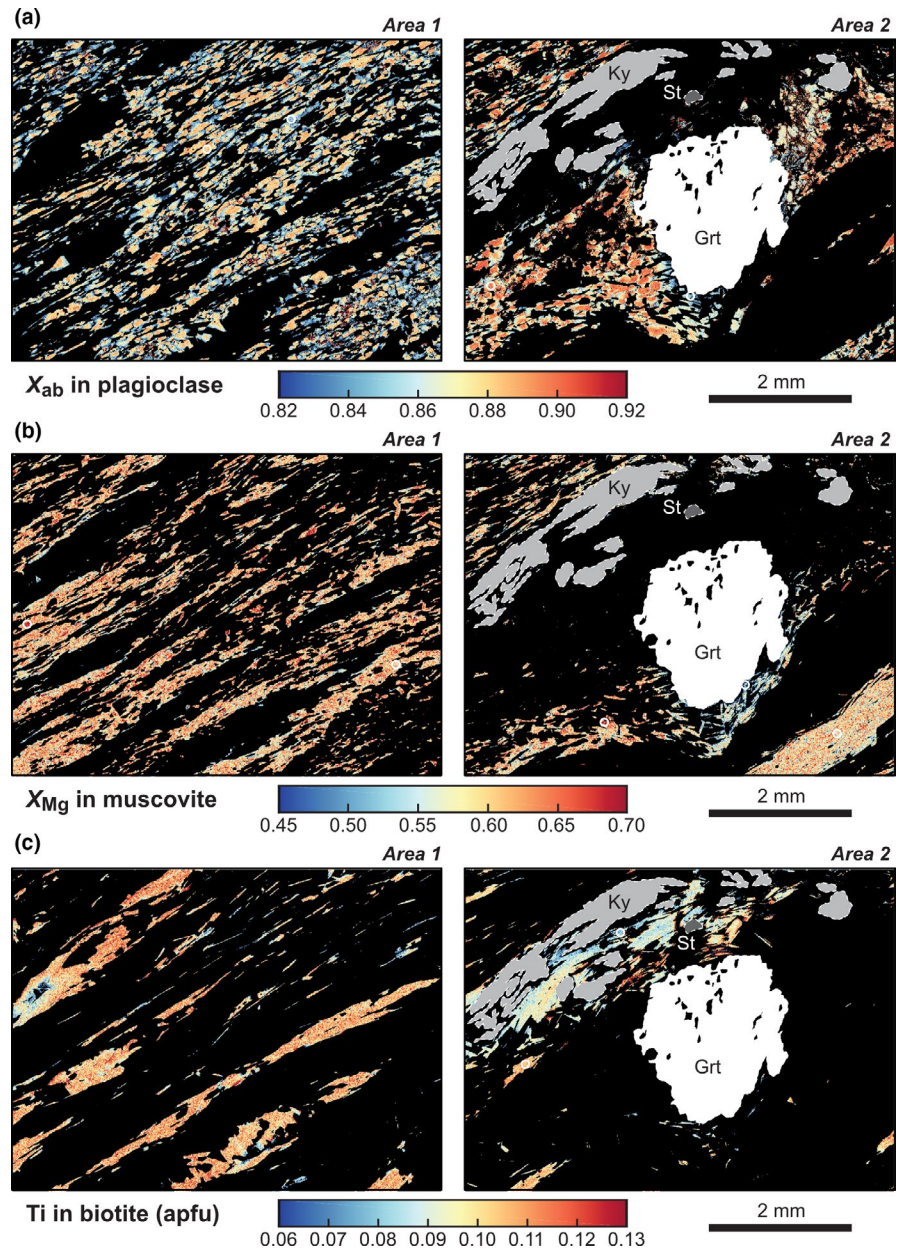
caused by diffusional modifications are described in the discussion. The diffusion length scale for Fe, Mg and Ca is evaluated at 100–300 μm assuming an original sharp boundary in composition between the mantle and the thin rim.

Plagioclase grains are compositionally zoned (Figure 8a) with slightly higher Na-content in cores (X_{ab} of 0.88–0.90) compared to rims ($X_{\text{ab}} \approx 0.85$). Plagioclase grains located within the pressure shadows of garnet have cores enriched in Na (up to X_{ab} of 0.91) compared to matrix grains (see also Material S3).

White mica exhibits a complex compositional zoning (Figure 8b) reflecting partial re-equilibration via pseudomorphic replacement (Airaghi, Lanari, de Sigoyer, & Guillot 2017; Santamaría-López, Lanari, & Sanz de Galdeano 2019). Patchy small phengite relics (Ph) have high Si contents and X_{Mg} (Si of 3.20–3.30 apfu; X_{Mg} of 0.65–0.71) and are surrounded by a single generation of muscovite (Ms_1) with lower Si contents and X_{Mg} (Si of 3.06–3.11 apfu; X_{Mg} of 0.60–0.62). A late generation of muscovite (Ms_2) is observed within the pressure shadow of garnet (Si ≈ 3.01 apfu; $X_{\text{Mg}} \approx 0.51$). The Na content continuously increases from Ph (0.08–0.15 apfu) to Ms_2 (0.22 apfu).

Biotite exhibits minor compositional zoning in the mineral matrix with Si and Ti contents of 2.74 ± 0.05 apfu and 0.11 ± 0.01 apfu respectively and X_{Mg} of 0.56 ± 0.02 (Bt_1). By contrast, the biotite grains located near kyanite and staurolite in the surrounding of garnet (Bt_2) have lower Ti (0.07 ± 0.03 apfu, see Figure 8c) for similar Si content and X_{Mg} . The second biotite generation (Bt_2) is systematically surrounded by chlorite (Figure 6d) suggesting partial retrograde re-equilibration at lower temperature conditions.

FIGURE 8 Quantitative compositional maps of (a) the albite fraction in plagioclase (b) the X_{Mg} corresponding to $Mg/(Mg+Fe^{2+})$ in muscovite and (c) the Ti-content in biotite (apfu) in areas 1 and 2. The location of garnet, kyanite and staurolite is marked with different grey levels in Area 2



3.4 | Petrographic interpretations

Based on the petrography, the compositional mapping and the statistical evaluation of the mineral compositions at least three stages of mineral equilibration can be postulated. Figure 9 shows the relative sequence of mineral formation/equilibration with respect to the main foliation. The prograde, synkinematic assemblage is characterized by Ab-rich plagioclase, white mica (both Ph_1 and Ms_1), biotite and garnet. Kyanite appears syn- to post-kinematic and is interpreted to form close to peak conditions. Ilmenite is present as inclusions in garnet, while rutile is aligned along the foliation and partly replaced by a second generation of ilmenite. Allanite was found as inclusion in garnet, while monazite is exclusively present in the mineral matrix. Staurolite overgrows the foliation, partly replaces kyanite and is occasionally in textural equilibrium with chlorite. Therefore,

staurolite is interpreted to represent a post-peak phase. Chlorite, Ms_2 and bt_2 partly replace other minerals and are considered of retrograde origin.

Apart from quartz and kyanite, the rock-forming minerals of this metapelite sample all exhibit compositional zoning. This observation already demonstrates that the rock was not fully re-equilibrated for major elements and key minor elements at the peak conditions reached during Alpine metamorphism (corresponding *sensu stricto* to T_{max} , the maximal temperature). Garnet, plagioclase and white mica exhibit variable chemical compositions between grain interiors and rims. Garnet fractionation during mineral growth is known to affect the reactive bulk composition (e.g. fractionation models by Evans, 2004; Gaidies, Capitani, & Abart 2008; Konrad-Schmolke, O'Brien, de Capitani, & Carswell 2008; Lanari & Engi, 2017) and therefore the position of isopleths in P - T

Stage \ Mineral	Prograde	Peak	Retrograde
	Foliation →		
Plagioclase	Ab ₈₉	Ab ₈₅	Ab ₉₁
Garnet	1	2	3 4
White mica	Si _{3.08}		Si _{3.01}
Biotite		Ti _{0.11}	Ti _{0.07}
Kyanite		—	
Staurolite		?
Chlorite			—
Ilmenite	—	
Rutile		
Allanite	—	
Monazite		

FIGURE 9 Classical crystallization-deformation diagram for the sample MA9330 from Todd and Engi (1997) and Boston et al. (2017)

isochemical phase diagrams (Spear, 1988a). Plagioclase fractionation is expected to produce similar deviations (Lanari & Duesterhoeft, 2019), whereas muscovite fractionation is usually negligible for isopleth thermobarometry (Airaghi et al., 2017; Santamaría-López et al., 2019).

3.5 | Phase equilibria

3.5.1 | Thermodynamic data and modelling programs

The thermodynamic models presented in the following are all based on the internally consistent data set of Holland and Powell (1998) and further updates collected in the Theriak-Domino database TC55_Bt distributed with Bingo-Antidote. The following solution models were used for feldspar (based on Baldwin, Powell, Brown, Moraes, & Fuck 2005; Holland & Powell, 2003); biotite (Tajčmanová, Connolly, & Cesare 2009); ilmenite, orthopyroxene, melt (White, Powell, & Holland, 2007); white mica (Coggon & Holland, 2002); chlorite (Holland, Baker, & Powell 1998); amphibole (Diener & Powell, 2012); garnet, staurolite, cordierite, epidote (Holland & Powell, 1998). The database TC55_Bt is the most robust database available to model the equilibrium relationships between garnet and biotite in amphibolite facies metapelites; the choice of this database is critical as the purpose of this work is to discuss possible equilibrium relationships between these two minerals.

The equilibrium phase diagrams were generated using THERIAK-DOMINO (de Capitani & Brown, 1987; De Capitani & Petrakakis, 2010) and ITM using BINGO-ANTIDOTE integrated in the XMAPTOOLS add-on XTHERMOTOOLS 1.2.1 (Duesterhoeft & Lanari, 2020). Garnet growth was simulated

using the computer program GRTMOD 1.6 that optimizes the reactive bulk composition used to model each growth stage of garnet (Lanari et al., 2017). The same database was used for GEM within each software package.

3.5.2 | Isochemical phase diagram based on the bulk rock composition

The P - T isochemical phase diagram of sample MA9330 is presented in Figure 10. This diagram was computed using the bulk rock composition determined by XRF reported in Boston (2014) and provided in Table 2. The observed mineral association (Bt+Ms+Pl+Grt+Ky+St+Ilm+St) is modelled in a narrow stability field at 620–630°C and 0.6–0.8 GPa (coloured in red in Figure 10) corresponding to the conditions obtained by Todd and Engi (1997). However, at these conditions, none of the modelled mineral compositions match the measured compositions (see summary in Table 3). This result suggests that at least one mineral phase was not part of the peak assemblage (Lanari & Duesterhoeft, 2019). The isochemical phase diagram based on the bulk rock composition cannot be directly used for this sample to estimate the peak conditions as it fails to reproduce the observations to a satisfactory level.

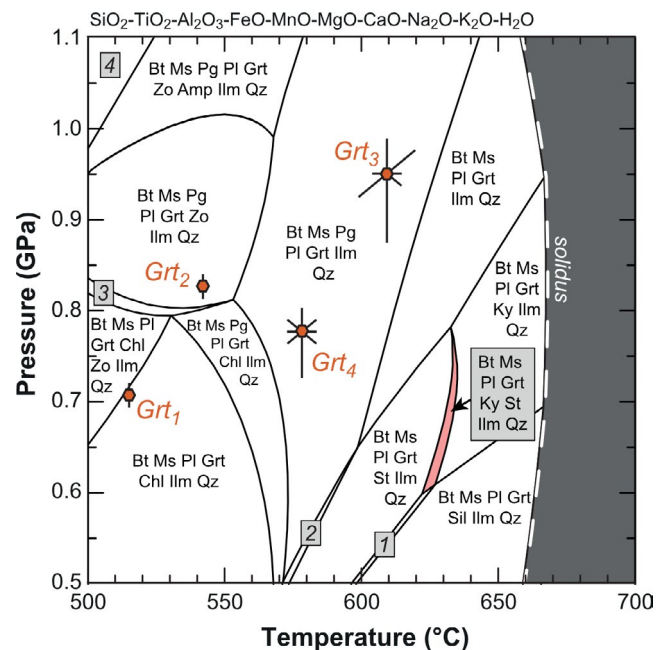


FIGURE 10 P - T phase diagram (also known as pseudosection) calculated for the bulk rock composition of sample MA9330. The inferred peak assemblage is underlined in red (see text for details). The orange dots mark the optimal solution for each growth zone of garnet (Grt₁, Grt₂, Grt₃ and Grt₄, see Figure 7) obtained using GRTMOD. Other stability fields: (1) Bt Ms Pl Grt St Sill Ilm Qz; (2) Bt Ms Pl Grt St Chl Ilm Qz; (3) Bt Ms Pg Pl Grt Chl Zo Ilm Qz; (4) Ms Pg Pl Grt Zo Amp Ilm Qz

TABLE 2 Bulk rock composition and local bulk compositions (LBC) of sample MA9330

	Bulk rock	LBC1.1	LBC2.1	LBC2.2
	XRF	Maps	Maps	Maps
	Boston (2014)	This study	This study	This study
Al ₂ O ₃	18.7	23.4	19.7	20.2
CaO	0.94	1.11	1.26	1.90
FeO	4.92	3.40	8.76	16.63
K ₂ O	3.81	4.57	2.24	1.97
MgO	1.82	2.37	2.54	4.28
MnO	0.10	0.00	0.19	0.37
Na ₂ O	2.08	4.26	2.09	1.27
SiO ₂	63.8	54.8	59.2	49.3
TiO ₂	0.76	0.68	0.46	0.58
Total	96.9	94.5	96.5	96.5

3.5.3 | Garnet modelling using GRTMOD

The P – T conditions of garnet growth were retrieved for four successive growth stages (Grt_{1–4} see Figure 7) assuming limited post-growth compositional modification by intracrystalline diffusion. The first garnet generation—modelled using the composition of garnet core Grt₁—is predicted to occur at 520°C and 0.71 GPa (Figure 10). As the second stage (Grt₂) is modelled at slightly higher P – T conditions (545°C and 0.82 GPa) the core–mantle zoning defines a prograde trajectory. The inner garnet rim (Grt₃) is modelled at 609°C and 0.95 GPa whereas the second rim (Grt₄) was modelled at 578°C and 0.77 GPa and involved resorption of 88% of Grt₃ from 3.08 to 0.35 vol.%. A total of 4.12 vol.% of garnet was simulated for this rock at the peak conditions based on the bulk rock composition, taking into account the progressive fractionation. No garnet resorption was modelled between Grt₁ and Grt₃. None of the solutions obtained for garnet growth (Grt_{1–3}) and resorption (Grt₄) stages overlap with the narrow stability field of the isochemical phase diagram representing the mineral association observed in this sample (Figure 10).

3.5.4 | ITM using BINGO-ANTIDOTE

Three areas-of-interest were investigated using BINGO-ANTIDOTE (see LBC-1.1, LBC-2.1 and LBC-2.2 in Figure 6). The geometry and size of each domain are arbitrary but minor variations in shape only result in minor deviations in the LBC and therefore in the thermodynamic model (Lanari & Engi, 2017). Large variations in the shape of the area-of-interest for the mineral matrix and around a garnet porphyroblast are further investigated in the discussion. The detailed results of each simulation are provided in Appendix 1.

The first area-of-interest (LBC-1.1 in Figure 6 and Table 2) samples the mineral matrix, which exhibits the mineral assemblage Pl+Ms+Bt+Qz+Ilm. This assemblage is modelled for the LBC LBC-1.1 in a large stability field between 550–650°C and 0.5–1 GPa (Figure 11a). Assuming that chemical equilibrium was achieved to a satisfactory degree with the plagioclase rims (Pl₂), the optimal P – T conditions derived by minimizing $-Q_{\text{total}}$ using *Recipe #1* of ANTIDOTE (*Find optimal P – T (-X)*) are 593°C and 0.65 GPa (Figure 11a). As the objective function is relatively flat within this stability field with variation lower than 3%, the associated uncertainties are at least $\pm 30^\circ\text{C}$ and 0.65 GPa. At these conditions, Q_{vol} is 95.6% and Q_{cmp} is 88.7%. Pressure–temperature maps of model-quality factor for biotite, muscovite (Ms₁), plagioclase core (Pl₁) and rim (Pl₂) are shown in Figure 11c–f. Whereas biotite and plagioclase rim are better modelled at $\sim 600^\circ\text{C}$ and 0.65 GPa, both plagioclase core and muscovite indicates higher pressure and lower temperature conditions between 520°C–0.85 GPa and 580°C–1.1 GPa. The Q_{cmp} values for biotite do not exceed 80% in the investigated P – T space.

The second area-of-interest (LBC-2.1 in Figure 6 and Table 2) samples the outer garnet rim (Grt₄) and the surrounding minerals. The inferred peak mineral assemblage is Grt+Bt+Pl+Ms+K+Qz+Ilm; both St and Chl are assumed to have formed later on upon exhumation and/or cooling (see Figure 9). This peak mineral assemblage is modelled for LBC-2.1 within a narrow stability field at 650°C and 0.9 GPa (Figure 12a). Assuming chemical equilibrium, optimal conditions were obtained at 664°C and 0.94 GPa with Q_{vol} of 95.4 and Q_{cmp} of 83.2%. Individual mineral P – T maps of Q_{cmp} exhibit a higher degree of complexity. Both biotite and muscovite show domains with higher Q_{cmp} values at lower temperatures for similar pressure conditions (520–560°C for Ms; 580–640°C for Bt). Only plagioclase rims (Pl₂) show high Q_{cmp} values in the stability field of the inferred peak mineral assemblage. Garnet rim (Grt₄) exhibits low Q_{cmp} values of $\sim 40\%$ in this stability field and rather records lower P – T conditions at 550°C and 0.7 GPa. In this model, the Q_{cmp} values of biotite are also systematically lower than 80%.

The third area-of-interest (LBC-2.2 in Figure 6 and Table 2) samples the garnet outer rim (Grt₄) and the associated retrograde phases located in the vicinity of garnet. In this case, the pixels of kyanite, muscovite, rutile and apatite were not considered for calculating LBC-2.2 as they are assumed to have formed at higher P – T conditions. The retrograde assemblage Grt+Bt+Chl+Pl+Ilm+Qz is modelled at 560–610°C and 0.5–0.7 GPa (Figure 13a). Assuming chemical equilibrium, optimal conditions were obtained at 597°C and 0.67 GPa with Q_{vol} of 93.2% and Q_{cmp} of 63.5%. The lower value of Q_{cmp} reflects a large mismatch in the mineral compositions also visible in the P – T maps of Q_{cmp} of individual minerals (Figure 13d–f). The conditions of highest Q_{cmp} value are 575°C–0.72 GPa for garnet, 580°C–0.8 GPa

TABLE 3 Observed (italic) and modeled (roman) mineral compositions

	Biotite				K-white mica			
	<i>T</i> (°C)	<i>P</i> (Gpa)	Si (apfu)	X_{Mg}	Ti (apfu)	Si (apfu)	X_{Mg}	Na (apfu)
<i>Prograde</i>						<i>3.29 ± 0.07</i>	<i>0.64 ± 0.07</i>	<i>0.09 ± 0.07</i>
<i>P</i> _{max}						<i>3.07 ± 0.10</i>	<i>0.60 ± 0.07</i>	<i>0.17 ± 0.07</i>
<i>T</i> _{max}			<i>2.77 ± 0.05</i>	<i>0.56 ± 0.02</i>	<i>0.13 ± 0.03</i>	<i>3.01 ± 0.05</i>	<i>0.50 ± 0.06</i>	<i>0.22 ± 0.08</i>
<i>Retrograde</i>			<i>2.78 ± 0.05</i>	<i>0.54 ± 0.02</i>	<i>0.05 ± 0.02</i>			
IPD (bulk)	629	0.65	2.48	0.45	0.14	3.03	0.54	0.25
IPD (bulk)	600	1.05	2.76	0.54	0.11	3.09	0.59	0.22
LBC1.1	540	0.96	2.87	0.6	0.09	3.14	0.65	0.16
Prograde								
LBC1.1 <i>T</i> _{max}	620	0.96	2.68	0.59	0.13	3.06	0.64	0.28
LBC1.1 Optimal	593	0.65	2.61	0.59	0.12	3.03	0.66	0.28
LBC2.1	540	0.96	2.83	0.42	0.09	3.12	0.5	0.17
Prograde								
LBC2.1 <i>T</i> _{max}	620	0.96	2.67	0.57	0.12	3.06	0.62	0.28
LBC2.1 Optimal	664	0.95	2.57	0.55	0.15	3.05	0.61	0.26
LBC2.2 Optimal	597	0.67	2.57	0.49	0.11	n.s.	n.s.	n.s.

Abbreviation: n.s. not predicted to be stable.

or 640°C–1.0 GPa for biotite, 600°C–0.7 GPa for staurolite and ~600°C–0.6 kbar for chlorite. Chlorite and biotite Q_{cmp} values do not exceed 65% and 80%.

4 | DISCUSSION

4.1 | *P*–*T* path of Croveo schists and mineral reaction sequence

The compositions preserved in minerals from the Croveo schist record at least three distinct metamorphic stages associated respectively to prograde, peak and retrograde Alpine metamorphism. As several minerals or part of minerals were not fully re-equilibrated at the peak conditions, a simple isochemical phase diagram cannot be used for thermobarometry. The main results obtained for each model are summarized in Figure 14a–c and discussed below; the synthetic *P*–*T* path is shown in Figure 14d.

4.2 | Stage 1—prograde metamorphism

Compositional record of prograde metamorphism is apparently preserved in garnet (Grt₁ and Grt₂), plagioclase interiors (Pl₁) and muscovite (Ms₁). The groups Ms₁ and Pl₁ define a prograde trajectory between 500°C–0.8 GPa and 580°C–1.1 GPa (Figure 14a,b,d) in model LBC1.1 corresponding to the mineral matrix. Similar conditions were obtained for muscovite in model LBC2.1 corresponding to the kyanite domain.

Garnet growth modelled using GrtMod is predicted to occur along a similar *P*–*T* gradient but at slightly higher temperatures or lower pressures (~40°C/~0.1 GPa in Figure 14a). These differences can either reflect minor inconsistencies in the thermodynamic data of garnet and plagioclase, or post-growth compositional modifications by intracrystalline diffusion (Lanari & Duisterhoeft, 2019). Diffusion of Fe, Mg, Mn and Ca in garnet is known to be efficient at temperature higher than 600°C (Caddick et al., 2010). The region, from which the studied sample was taken, stayed at temperatures above 600°C for up to 10 Myr (see below). Therefore, some diffusion of divalent cations in garnet is expected. By contrast, diffusion of Fe–Mg in phengite and Na–Ca in plagioclase are rather sluggish at these conditions. The exchange in plagioclase (CaAlNa₁Si₁) and phengite (MgSiAl₂) both involve coupled substitutions involving a Si-site. This explains why prograde features in these two minerals are so well preserved. The comparison between garnet profiles modelled along the two trajectories suggests that the shift of 40°C towards higher temperature could be related to post-growth compositional changes driven by intragranular diffusion in garnet. The resulting changes in end-member fractions are lower than 0.07 for Fe, and Ca; lower than 0.02 for Mg and Mn, in line with the range of absolute end-member fractions. No attempt of diffusion modelling was made in this study due to the complexity of the compositional zoning related to the presence of a large quantity of mineral inclusions (see Figure 7 and Material S2). In this case, we simply infer that the *P*–*T* conditions obtained using the observed garnet compositions do not reflect growth conditions. A narrow range of rutile formation

Plagioclase			Staurolite	Garnet			
Na (apfu)	Ca (apfu)	K (apfu)	X_{Mg}	X_{alm}	X_{prp}	X_{grs}	X_{sps}
0.89 ± 0.02	0.09 ± 0.01	0.01 ± 0.01		0.48 ± 0.02	0.04 ± 0.01	0.27 ± 0.01	0.19 ± 0.01
				0.59 ± 0.02	0.04 ± 0.01	0.27 ± 0.02	0.08 ± 0.01
0.85 ± 0.01	0.14 ± 0.01	0.01 ± 0.01	0.22 ± 0.02	0.75 ± 0.02	0.08 ± 0.01	0.14 ± 0.02	0.02 ± 0.01
0.76	0.23	0.01	0.15	0.71	0.13	0.05	0.1
0.8	0.19	0.01	n.s.	0.65	0.11	0.2	0.03
0.88	0.11	0.01	n.s.	n.s.			
0.84	0.15	0.01	n.s.	n.s.			
0.84	0.14	0.02	n.s.	n.s.			
n.s.	n.s.	n.s.	n.s.	0.62	0.05	0.3	0.03
0.76	0.23	0.01	n.s.	0.66	0.15	0.17	0.02
0.82	0.17	0.01	n.s.	0.71	0.2	0.07	0.02
0.71	0.28	0.01	0.15	0.74	0.14	0.08	0.02

temperatures was obtained by Boston et al. (2017) using Zr-in-rutile thermometry for rutile crystals of the same sample; they indicate prograde rutile growth at $\sim 570^\circ\text{C}$ at a pressure of 1.05 GPa (Figure 14). In the model, rutile is only predicted to be stable at higher pressure conditions (>1.1 GPa). In any case, the appearance of rutile prior to the peak temperature stage suggests that peak pressure stage preceded the peak metamorphic stage 2.

4.3 | Stage 2—peak metamorphism

The equilibrium relationships related to the metamorphic peak are also challenging to establish. An attempt is made below based on a combination of results obtained using GRTMOD and BINGO-ANTIDOTE for the kyanite domain and the mineral matrix. Firstly, the inner rim of garnet was modelled by GRTMOD at 609°C and 0.95 GPa (Grt₃ in Figure 10). As this garnet composition is not present in LBC2.1 (kyanite domain), it cannot be modelled in BINGO-ANTIDOTE. In these models, the geometry of the kyanite stability field varies depending on the LBC, but systematically indicates temperatures above 620°C for pressures ranging between 0.6 and 1 GPa. The phase diagram computed for LBC2.1 (kyanite domain) exhibits a larger kyanite stability field for pressures above 0.8 GPa compared to the models based on the bulk rock composition or for the mineral matrix (Figure 14d). The shift of the kyanite-in reaction towards lower temperatures in model LBC2.1 could explain why kyanite nucleation was favoured in the vicinity of the

garnet porphyroblasts (Figure 6). The LBC could have been more favourable for kyanite nucleation to occur at lower P – T conditions. Interestingly, kyanite is predicted to be stable in all models at the optimal solution for peak metamorphism obtained for the kyanite domain (664°C and 0.94 GPa; red star in Figure 14b). By contrast, the composition of biotite and plagioclase (Pl_2) in the mineral matrix and in the kyanite domain combined with Ti-in-biotite thermometry indicate slightly lower peak conditions at 620°C for a similar pressure of 0.9 GPa (red star labelled ‘peak’ in Figure 14d). This solution is favoured here as kyanite stability can be extended to lower temperature due to the incorporation of trace amounts of Fe^{3+} , which is not considered in the model. As Plagioclase is the only significant carrier of Ca in the mineral matrix, the optimal Q_{cmp} for plagioclase Pl_2 covers a broad area preventing determination of growth conditions with a high degree of confidence. It is instructive to compare this result with the approach of the equilibrium model (Figure 10). It is evident that the narrow field with the assumed peak assemblage is a poor match to the complex evolution based on the mapping approach.

4.4 | Stage 3—cooling and exhumation

The equilibrium relationships related to cooling and exhumation are observed in local domains, for example around the garnet porphyroblasts (Figure 6). The mineral matrix does not show any clear evidence of retrogression and chlorite is notably absent. Ti-in-biotite thermometry in biotite

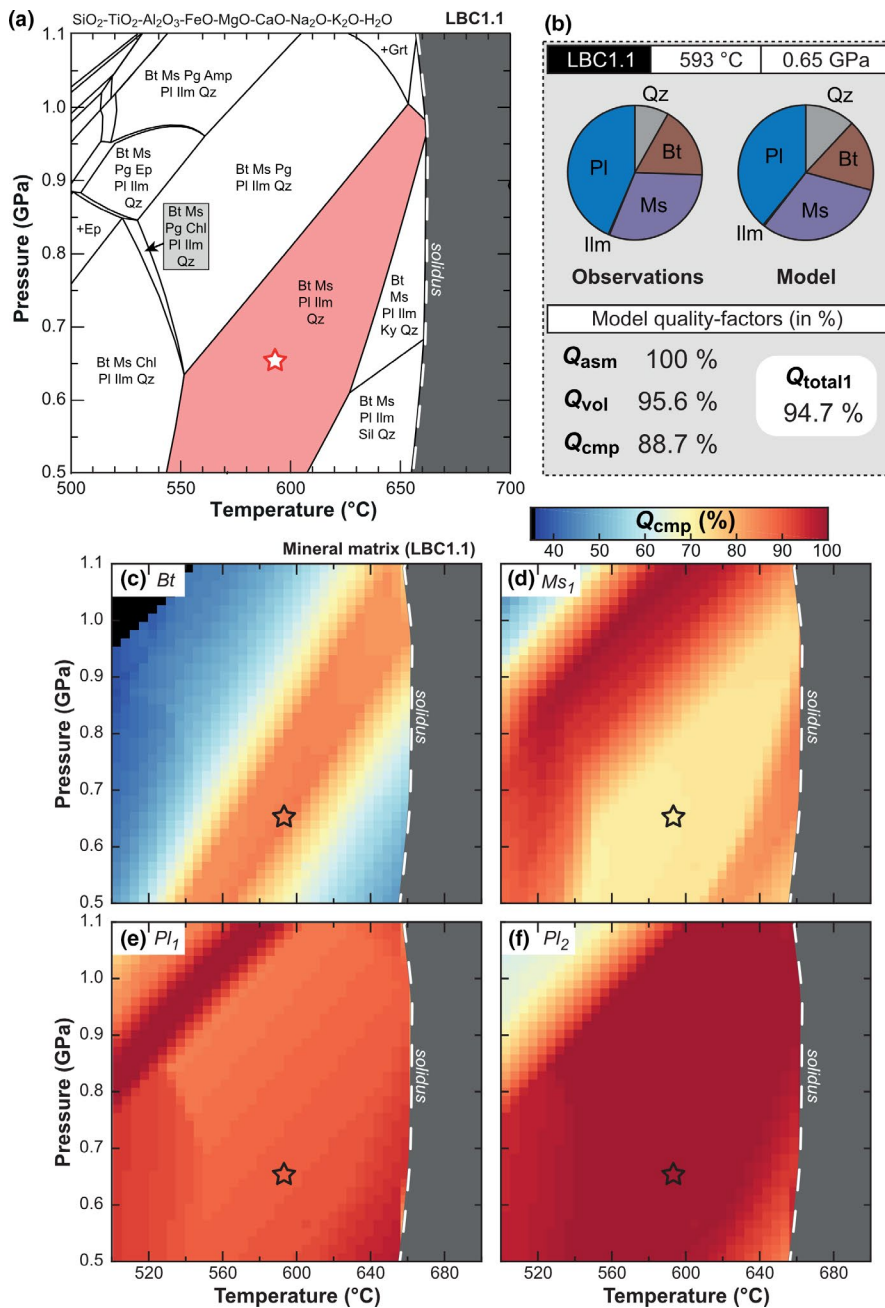


FIGURE 11 Results of ITM for the 'mineral matrix' based on LBC1.1. (a) P - T phase diagram. The red star shows the optimal solution obtained at 593°C and 0.65 GPa using ANTIDOTE (see text for details). (b) Observed/modelled mineral modes and quality factors for the optimal solution obtained with BINGO. (c) Map of quality-factor Q_{cmp} for biotite. (d) Map of quality-factor Q_{cmp} for muscovite. (e) Map of quality-factor Q_{cmp} for plagioclase core (Pl_1). (f) Map of quality-factor Q_{cmp} for plagioclase rim (Pl_2)

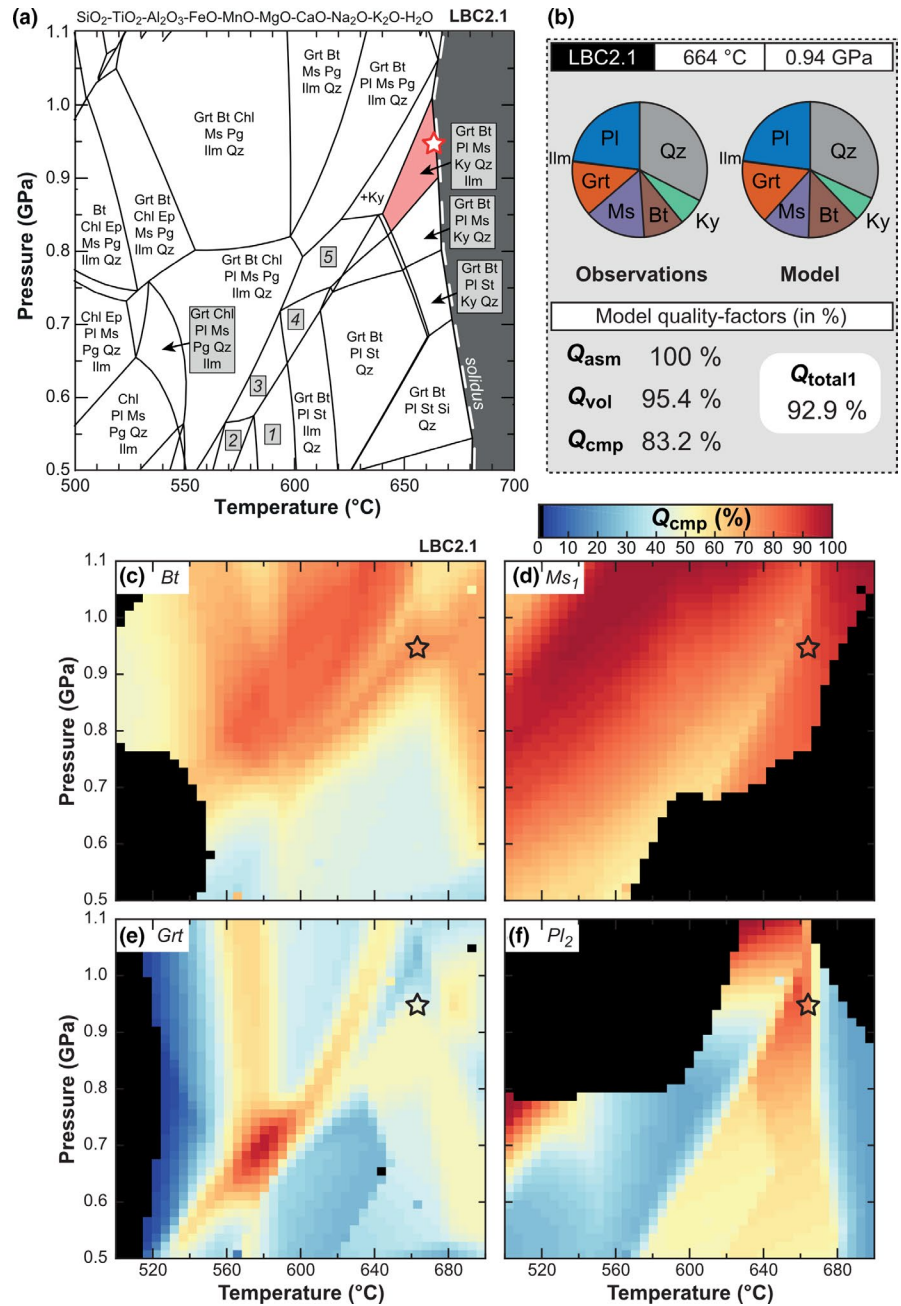
associated with chlorite in the kyanite domains indicates temperatures of $570 \pm 30^\circ\text{C}$ further supporting the retrograde character of the biotite associated to garnet rim (Gr_4), staurolite and chlorite (Figure 14c). Chlorite has an extended stability field if the equilibrium is local (compare Figure 10 and Figure 13a) with the chlorite out curve moving from $\sim 570^\circ\text{C}$ for the bulk rock composition to $\sim 620^\circ\text{C}$ in the retrogressed domain. In this case we can postulate that chlorite is more likely to form from a local reaction and eventually above the chl-out curve predicted for the bulk rock composition. The model for the kyanite zone (excluding kyanite and muscovite which were metastable) also suggests that chlorite and staurolite equilibrated—partially with biotite and garnet—at 600°C and 0.67 GPa (Figure 14d).

4.5 | Metastability—effects of phase proportions in the area-of-interest

The detailed petrological investigation based on quantitative compositional maps and ITM indicates that the Croveo Schist was only partially re-equilibrated at the peak conditions of 620°C and 0.9 GPa. In this case, the fraction of mineral relics used in the LBC can affect the model-quality factors as demonstrated for plagioclase in the theoretical example. Such effects are investigated below (a) for the mineral matrix and (b) for the kyanite domain.

In the mineral matrix, 51.1 vol.% of the minerals are interpreted as metastable at the peak conditions including plagioclase interiors (22.7% out of 43.3% of plagioclase),

FIGURE 12 Results of ITM for the ‘kyanite domain’ based on LBC2.1. (a) P – T phase diagram. The red star shows the optimal solution obtained at 664°C and 0.94 GPa using ANTIDOTE (see text for details). Mineral assemblages: (1) Grt Bt Chl Pl St Ilm Qz; (2) Bt Chl Ms Pl St Ilm Qz; (3) Grt Bt Ms Chl Pl St Ilm Qz; (4) Grt Bt Ms Pl St Ilm Qz; (5) Grt Bt Ms Pg Pl St Ilm Qz. (b) Observed/modelled mineral modes and quality factors for the optimal solution obtained with BINGO. (c) Map of quality-factor Q_{cmp} for biotite. (d) Map of quality-factor Q_{cmp} for muscovite. (e) Map of quality-factor Q_{cmp} for garnet (Grt₄). (f) Map of quality-factor Q_{cmp} for plagioclase rim (Pl₂)



muscovite (30.3%) and rutile (0.2%). This is quite astonishing, showing that even in a typical amphibolite facies metapelite, the assumption of thin-section wide equilibrium that would allow modelling using the measured bulk rock is not justified. While in the past there has been a lot of attention on the effect of zoned garnet on the reactive bulk composition (e.g. Evans, 2004; Lanari & Engi, 2017; Spear, 1988a), our study shows that phengite and plagioclase have abundant relics that are not easily equilibrated at peak conditions.

Sensitivity tests were performed at 593°C and 0.65 GPa for a total of 87 LBC including various phase proportions (see Figure 15) obtained using a combination of floating (*Recipe #10*), scanning (*Recipe #11*) and sliding (*Recipe*

#12) windows in ANTIDOTE (Duesterhoef & Lanari, 2020). Results are shown in Figure 15 based on the modelled mineral modes, which mimic the phase proportions used to calculate each LBC (e.g. Figure 11b). Minor changes in the Q_{cmp} value of minerals are observed—within 1% for plagioclase or biotite and within 10% for muscovite. By contrast, the values of Q_{total1} do not change significantly with the phase proportion (Figure 15d–f). In this example, the compositions of Pl₁ and Pl₂ are close (X_{ab} of 0.87–0.90 and 0.85 respectively) and do not influence significantly the results for simulations ranging between 30 and 50 vol.% of plagioclase. In addition, plagioclase is the only significant carrier of Ca and the main carrier of Na in the mineral matrix preventing large compositional changes caused by element partitioning. The

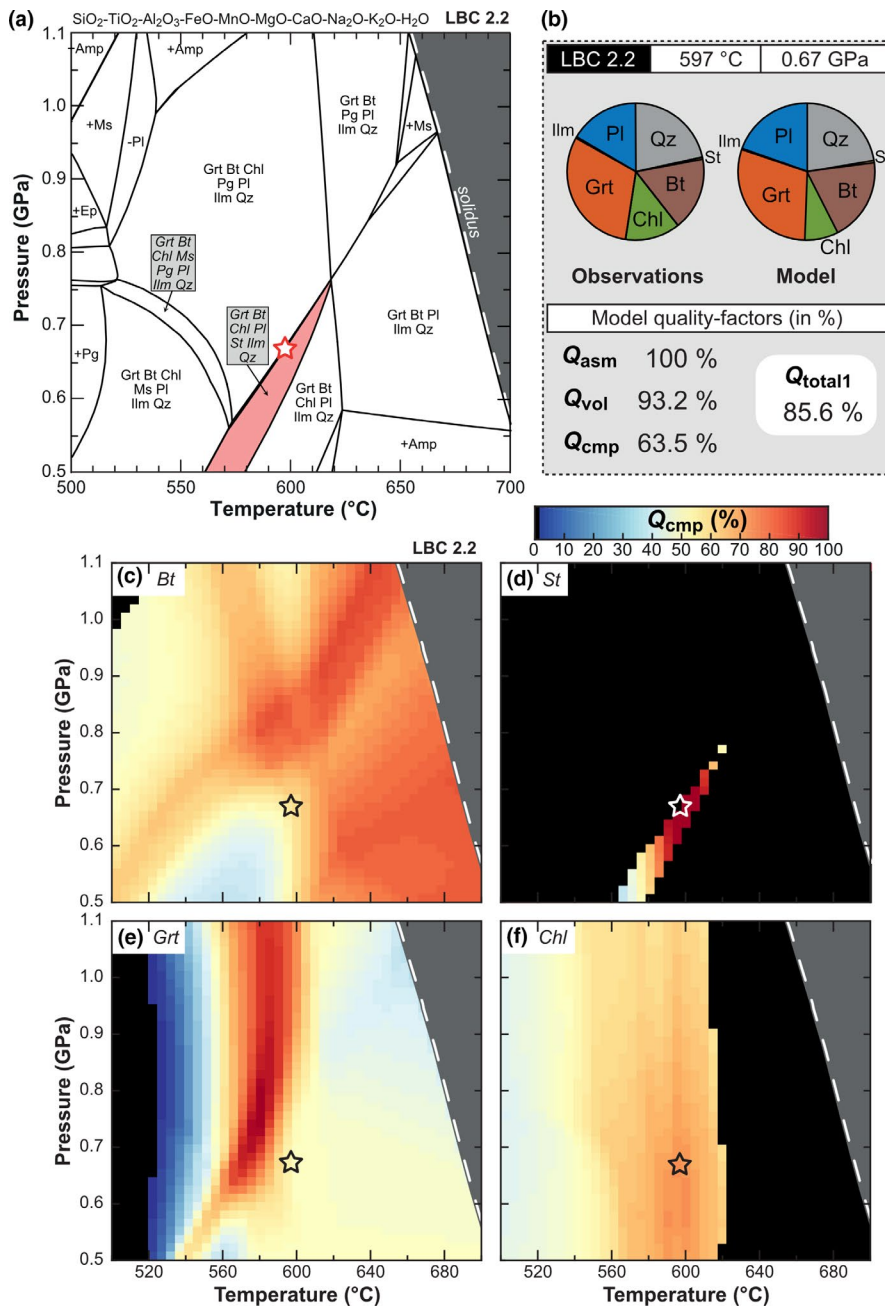


FIGURE 13 Results of ITM for the ‘retrogression’ based on LBC2.2. Note that kyanite and muscovite are not considered in this simulation (a) P - T phase diagram. The red star shows the optimal solution obtained at 597°C and 0.67 GPa using ANTIDOTE (see text for details). (b) Observed/modelled mineral modes and quality factors for the optimal solution obtained with BINGO. (c) Map of quality-factor Q_{cmp} for biotite. (d) Map of quality-factor Q_{cmp} for staurolite. (e) Map of quality-factor Q_{cmp} for garnet (Grt_4). (f) Map of quality-factor Q_{cmp} for chlorite

results of the simulation are also not sensitive to the fraction of muscovite and biotite. In this first example, metastable relicts cannot be identified only based on LBC with various phase proportions at fixed P - T conditions, as the value of Q_{total1} is not affected by the modes. For such high-variance assemblage, P - T maps of Q_{cmp} have proved to be more helpful (Figure 11 and its interpretation in Figure 14a).

In the kyanite domain (LBC2.1), 38.5 vol.% of the minerals are interpreted as metastable at the peak conditions or re-equilibrated thereafter including garnet (11.3 vol.%), plagioclase interiors (11.2% out of 22.4% of plagioclase), muscovite (15.9%) and rutile (0.9%). Sensitivity tests were performed at the optimal conditions obtained for LBC2.1 in the kyanite stability field (664°C and 0.94 GPa) for a total of 316 LBC including various

garnet volume fractions (Figure 16). In this second example, the fraction of garnet in the area-of-interest has a strong effect on the value of Q_{total1} . If more garnet is included in the LBC, the model quality is lower. The value of Q_{total1} is 84% for 45 vol.% of garnet and reaches 93.5% for <1 vol.% of garnet. Two trends are observed at low garnet fraction depending if the bulk is taken in the bottom right corner of the map (high muscovite, low biotite) and top left corner (low muscovite and high biotite). These results demonstrate that phase equilibrium modelling applied to local domains containing a high fraction of phases that were not in chemical equilibrium (such as the later re-equilibrated garnet rim Grt_4) can significantly affect the quality of the model predictions. Correlation between mineral modes and model-quality factors can serve to detect the presence of phases not in chemical

FIGURE 14 Synthetic P - T diagrams showing the optimal conditions derived for each compositional group of solid solutions based on the quality factors (Q_{comp}) shown in Figures 10–12. Additional thermobarometric constraints include: Zr-in-rutile data from Boston et al. (2017), Ti-in-biotite temperatures obtained using the calibration of Henry et al. (2005) (a) ‘mineral matrix’ based on LBC1.1. (b) Peak mineral assemblage based on LBC2.1. (c) Retrograde conditions based on LBC2.2. (d) Synthetic P - T path and mineral formation sequence. The alternative path for LBC2.1 (peak conditions) shown in a short-dashed line is based on the optimal peak conditions determined for this domain. The alternative path shown in a continuous line is interpreted as more robust for this stage (see text)

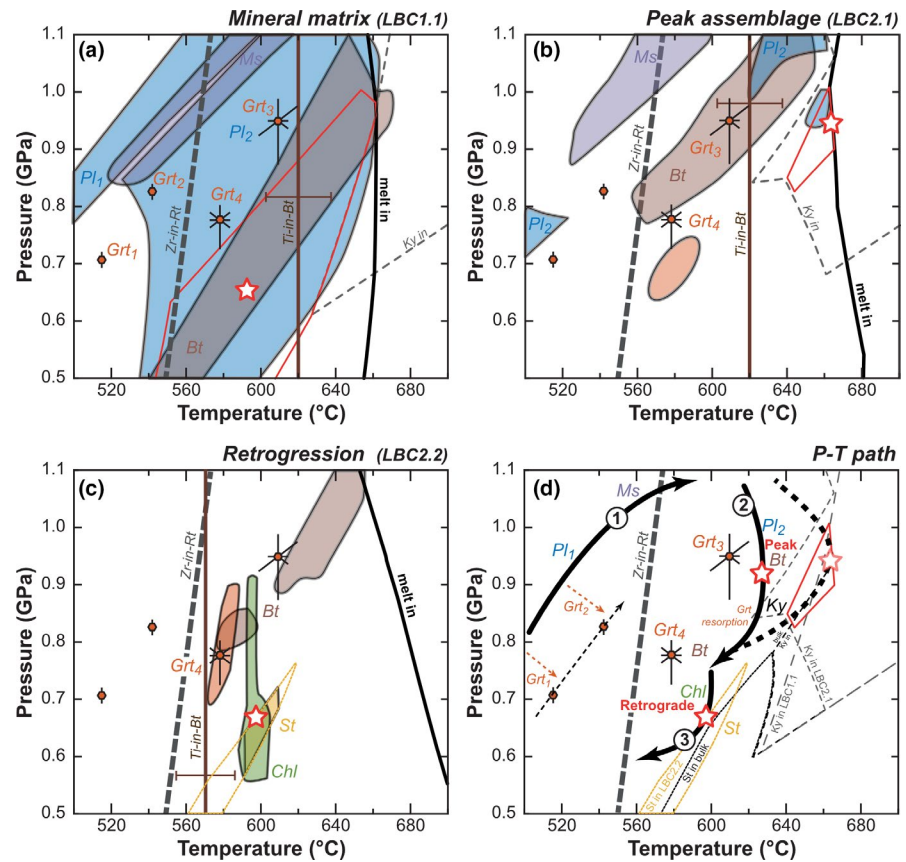
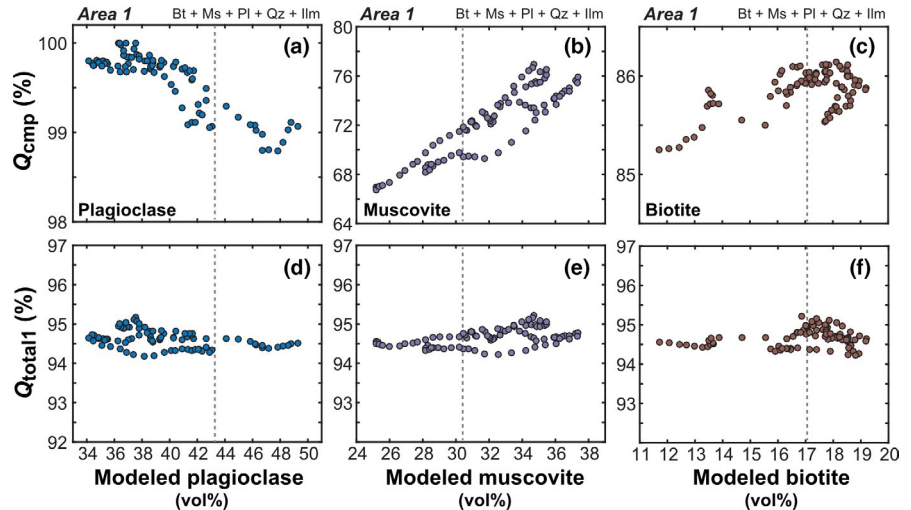


FIGURE 15 Effects of phase proportions in the area-of-interest on the model-quality factor for the mineral matrix (LBC1.1) modelled at 593°C and 0.65 GPa using 87 local bulk compositions with variable mineral modes



equilibrium at a given stage. In this example, the garnet rim was re-equilibrated during cooling.

4.6 | Interpretations of the P - T path followed by the Croveo schists

The conditions of prograde metamorphism recorded by the Croveo schists are documented in aligned, relic plagioclase and muscovite indicating recrystallization during deformation. Peak pressures are not very well constrained, as this

stage did not lead to a significant new mineral growth that is preserved. Nevertheless, with the mapping approach and the combination of the presence of rutile, Zr-in-rutile thermometry and the compositions of muscovite and plagioclase it is possible to retrieve pressures of ~1.0 to 1.1 GPa for the rocks, indicating burial to ~35 to 40 km depths. The Croveo schists come from a Mesozoic, metasedimentary cover that separates the Verampio gneiss dome from the overlying Antigorio nappe. They represent the lowest members in the nappe stack of the Central Alps that were derived from the European continental margin (Steck et al., 2013). The

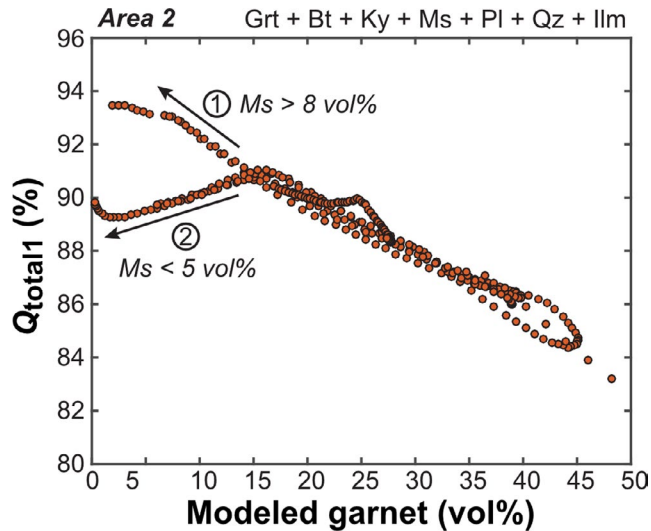


FIGURE 16 Effects of phase proportions in the area-of-interest on the model-quality factor for the kyanite domain (LBC2.1) modelled at 664°C and 0.94 GPa using 316 local bulk compositions with variable mineral modes

intermediate temperatures and elevated pressures of the prograde stage are thus likely associated with continental subduction and nappe stacking. A prograde pressure peak at 0.9–1.0 GPa has been proposed in Mesozoic metasediments in the Naret region (Galli et al., 2007) that separate the Lebedun from the Maggia nappe, in a similar tectonic position than the investigated sample (Steck et al., 2013). The timing of nappe stacking in the Central Alps is quite well constrained at ~32 to 27 Ma (Boston et al., 2017; Rubatto, Hermann, Berger, & Engi 2009).

Peak temperature conditions of ~620°C postdate peak pressure conditions and are associated with slightly lower pressures of ~0.9 GPa (Figure 14). These conditions are below the wet solidus, in agreement with the observation that no migmatization took place. Based on equilibrium phase diagrams, a similar peak pressure has been proposed for metapelites in the Naret and Campolungo regions to the North East, however, temperatures were slightly higher at ~650 to 670°C (Galli et al., 2007; Gieré, Rumble, Günther, Connolly, & Caddick 2011), both at conditions above the wet solidus. Using multiphase equilibria modelling, peak P – T conditions of Croveo metasediments were previously determined at 617°C ± 11°C and 0.62 GPa (Todd & Engi, 1997). The peak temperature stage is related to the classical mapped field gradient of Barrovian metamorphism in the Central Alps (Trommsdorff, 1966) that has been quantified in the isograds maps by Todd and Engi (1997). These isograds crosscut the nappe boundaries, providing clear evidence that Barrovian metamorphism outlasted the deformation related to the nappe stacking.

Peak metamorphic conditions were followed in the Croveo schists by a further amphibolite facies re-equilibration at slightly lower temperatures of 600°C but significantly

lower pressures of ~0.65 GPa. Monazite is only present in the matrix of the investigated sample and has been dated at 21.7 ± 0.4 Ma (Boston et al., 2017), likely representing the last stage of amphibolite facies metamorphism. The studied rock thus resided for 5–10 Ma at temperatures of 600 ± 20°C after the initial stage of nappe stacking. The modelling suggests that garnet compositions were affected by diffusion, modifying prograde garnet composition so that the apparent temperatures are higher for Grt₁ and Grt₂, but slightly lower for peak Grt₃ (Figure 14d). It is important to note that this shift towards higher apparent temperature could also be interpreted as a consequence of reaction overstepping. Although the topic has attracted a lot of attention in the recent years (Castro & Spear, 2017; Spear & Pattison, 2017; Spear, Thomas, & Hallett 2014), garnet reaction overstepping cannot be invoked (or quantified) in the present example as the mapped garnet porphyroblast was probably cut off centre; a hypothesis that can hardly be verified without the use of microtomography (e.g. George & Gaidies, 2017). As 0.5 vol.% of garnet is modelled by GrtMod using the composition of Grt₁, the centre of this grain could be located at least ~350 µm away assuming a spherical garnet geometry. The composition of initial garnet growth that could be used to retrieve the nucleation conditions is therefore unknown.

5 | CONCLUSIONS

This contribution reports two application examples of ITM applied to metapelitic systems.

The theoretical example based on an average pelite composition shows that the investigation of well-equilibrated samples via ITM can be performed using either the bulk rock composition or any LBC obtained from quantitative compositional maps. However, the interpretations must be restricted to the P – T conditions under investigation as stability fields are highly sensitive to variations in bulk composition. The investigation of samples with disequilibrium features such as metastable plagioclase (e.g. Lanari & Duesterhoeft, 2019) requires a special attention. The interpretation of modelled mineral assemblages can be ambiguous in the presence of relics that are predicted to be stable far away from their formation conditions. The phase(s) in disequilibrium can in theory be assessed from maps of quality factors for each mineral or statistically by combining LBC obtained from domains with variable mineral mode (Figure 4).

The natural example based on a metapelite (Croveo Schist) from the Central Alps showed that different parts of the thin section record several stages of a P – T path. The stability field of the inferred peak assemblage in a P – T phase diagram computed for the bulk rock composition is misleading as part of the minerals formed earlier during prograde metamorphism. These relics survived due to sluggish intragranular diffusion

at 620°C. A detailed P – T path was obtained based on three simulations using their respective LBC. The following stages were obtained: (a) prograde metamorphic conditions related to continental subduction are recorded by muscovite, plagioclase cores, garnet interiors and rutile; peak temperature conditions associated with the Alpine collision are documented by plagioclase rims, biotite and kyanite; retrograde conditions still within the amphibolite facies produced the local assemblage chlorite+staurolite±garnet (rim)±biotite. The effect of garnet re-equilibration by diffusion or replacement was simulated using LBC determined with various volume fractions of garnet rim. However, this technique cannot be applied to phases with minor compositional variability (plagioclase core and rim) or for phases that do not exchange diagnostic elements with other phases (muscovite). The proposed approach represents a way forward in combining detailed textural observations of multiple mineral growth in metamorphic rocks with compositional mapping and equilibrium thermodynamic modelling. This allows the determination of stable mineral assemblages and their compositions, which represents the fundamentals for the construction of robust P – T paths.

ACKNOWLEDGEMENTS

The authors acknowledge Daniela Rubatto for providing the sample MA9330 and for stimulating discussions regarding equilibrium/disequilibrium processes in metamorphic rocks as well as Erik Duesterhoeft for his comments on a preliminary version of this manuscript. Freya George and an anonymous reviewer are thanked for their constructive reviews that improved the presentation of the final paper. Katy Evans is thanked for providing suggestions and for her efficient editorial handling.

ORCID

Pierre Lanari  <https://orcid.org/0000-0001-8303-0771>

Jörg Hermann  <https://orcid.org/0000-0001-8360-3592>

REFERENCES

- Airaghi, L., Lanari, P., de Sigoyer, J., & Guillot, S. (2017). Microstructural vs compositional preservation and pseudomorphic replacement of muscovite in deformed metapelites from the Longmen Shan (Sichuan, China). *Lithos*, 282–283, 262–280. <https://doi.org/10.1016/j.lithos.2017.03.013>
- Baldwin, J. A., Powell, R., Brown, M., Moraes, R., & Fuck, R. A. (2005). Modelling of mineral equilibria in ultrahigh-temperature metamorphic rocks from the Anápolis-Itaçu Complex, central Brazil. *Journal of Metamorphic Geology*, 23(7), 511–531. <https://doi.org/10.1111/j.1525-1314.2005.00591.x>
- Berman, R. G. (1991). Thermobarometry using multi-equilibrium calculations: A new technique, with petrological applications. *Canadian Mineralogist*, 29, 833–855.
- Boston, K. R. (2014). Investigation of accessory allanite, monazite and rutile of the Barrovian sequence of the Central Alps (Switzerland). PhD thesis; The Australian National University.
- Boston, K. R., Rubatto, D., Hermann, J., Engi, M., & Amelin, Y. (2017). Geochronology of accessory allanite and monazite in the Barrovian metamorphic sequence of the Central Alps, Switzerland. *Lithos*, 286–287, 502–518. <https://doi.org/10.1016/j.lithos.2017.06.025>
- Brown, T. H., & Skinner, B. J. (1974). Theoretical prediction of equilibrium phase assemblages in multicomponent systems. *American Journal of Science*, 274(9), 961–986. <https://doi.org/10.2475/ajs.274.9.961>
- Caddick, M. J., Konopásek, J., & Thompson, A. B. (2010). Preservation of garnet growth zoning and the duration of prograde metamorphism. *Journal of Petrology*, 51(11), 2327–2347. <https://doi.org/10.1093/ptrology/egq059>
- Castro, A. E., & Spear, F. S. (2017). Reaction overstepping and re-evaluation of peak P-T conditions of the blueschist unit Sifnos, Greece: Implications for the Cyclades subduction zone. *International Geology Review*, 59(5–6), 548–562. <https://doi.org/10.1080/00206814.2016.1200499>
- Ceccato, A., Goncalves, P., & Pennacchioni, G. (2020). Temperature, fluid content and rheology of localized ductile shear zones in sub-solidus cooling plutons. *Journal of Metamorphic Geology*, 38(8), 881–903. <https://doi.org/10.1111/jmg.12553>
- Coggon, R., & Holland, T. J. B. (2002). Mixing properties of phengitic micas and revised garnet-phengite thermobarometers. *Journal of Metamorphic Geology*, 20(7), 683–696. <https://doi.org/10.1046/j.1525-1314.2002.00395.x>
- Connolly, J. A. D., & Kerrick, D. M. (1987). An algorithm and computer program for calculating composition phase diagrams. *Calphad*, 11(1), 1–55. [https://doi.org/10.1016/0364-5916\(87\)90018-6](https://doi.org/10.1016/0364-5916(87)90018-6)
- de Capitani, C., & Brown, T. H. (1987). The computation of chemical equilibrium in complex systems containing non-ideal solutions. *Geochimica et Cosmochimica Acta*, 51(10), 2639–2652. [https://doi.org/10.1016/0016-7037\(87\)90145-1](https://doi.org/10.1016/0016-7037(87)90145-1)
- De Capitani, C., & Petrakakis, K. (2010). The computation of equilibrium assemblage diagrams with Theriak/Domino software. *American Mineralogist*, 95(7), 1006–1016. <https://doi.org/10.2138/am.2010.3354>
- Di Rosa, M., De Giorgi, A., Marroni, M., & Vidal, O. (2017). Syn-convergence exhumation of continental crust: Evidence from structural and metamorphic analysis of the Monte Cecu area, Alpine Corsica (Northern Corsica, France). *Geological Journal*, 52(6), 919–937. <https://doi.org/10.1002/gj.2857>
- Diener, J. F. A., & Powell, R. (2012). Revised activity-composition models for clinopyroxene and amphibole. *Journal of Metamorphic Geology*, 30(2), 131–142. <https://doi.org/10.1111/j.1525-1314.2011.00959.x>
- Duesterhoeft, E., & Lanari, P. (2020). Iterative thermodynamic modelling—Part 1: A theoretical scoring technique and a computer program (Bingo-Antidote). *Journal of Metamorphic Geology*, 38, 527–551. <https://doi.org/10.1111/jmg.12538>
- Engi, M., Lanari, P., & Kohn, M. J. (2017). Significant ages—An introduction to petrochronology. *Methods and Applications*, 83, 1–12. <https://doi.org/10.2138/rmg.2017.83.1>
- Evans, T. P. (2004). A method for calculating effective bulk composition modification due to crystal fractionation in garnet-bearing schist: Implications for isopleth thermobarometry. *Journal of Metamorphic Geology*, 22(6), 547–557. <https://doi.org/10.1111/j.1525-1314.2004.00532.x>
- Gaidies, F., Capitani, C., & Abart, R. (2008). THERIA_G: A software program to numerically model prograde garnet growth.

- Contributions to Mineralogy and Petrology*, 155(5), 657–671. <https://doi.org/10.1007/s00410-007-0263-z>
- Galli, A., Mancktelow, N., Reusser, E., & Caddick, M. (2007). Structural geology and petrography of the Naret region (northern Valle Maggia, N. Ticino, Switzerland). *Swiss Journal of Geosciences*, 100(1), 53–70. <https://doi.org/10.1007/s00015-007-1211-7>
- George, F. R., & Gaidies, F. (2017). Characterisation of a garnet population from the Sikkim Himalaya: Insights into the rates and mechanisms of porphyroblast crystallisation. *Contributions to Mineralogy and Petrology*, 172(7), 57. <https://doi.org/10.1007/s00410-017-1372-y>
- Gieré, R., Rumble, D., Günther, D., Connolly, J., & Caddick, M. J. (2011). Correlation of growth and breakdown of major and accessory minerals in metapelites from Campolungo, Central Alps. *Journal of Petrology*, 52(12), 2293–2334. <https://doi.org/10.1093/ptrology/egr043>
- Guevara, V. E., & Caddick, M. J. (2016). Shooting at a moving target: Phase equilibria modelling of high-temperature metamorphism. *Journal of Metamorphic Geology*, 34(3), 209–235. <https://doi.org/10.1111/jmg.12179>
- Henry, D. J., Guidotti, C. V., & Thomson, J. A. (2005). The Ti-saturation surface for low-to-medium pressure metapelitic biotites: Implications for geothermometry and Ti-substitution mechanisms. *American Mineralogist*, 90(2–3), 316–328. <https://doi.org/10.2138/am.2005.1498>
- Hensen, B. J. (1971). Theoretical phase relations involving cordierite and garnet in the system MgO-FeO-Al₂O₃-SiO₂. *Contributions to Mineralogy and Petrology*, 33(3), 191–214. <https://doi.org/10.1007/BF00374063>
- Holland, T., Baker, J., & Powell, R. (1998). Mixing properties and activity-composition relationships of chlorites in the system MgO-FeO-Al₂O₃-SiO₂-H₂O. *European Journal of Mineralogy*, 10(3), 395–406. <https://doi.org/10.1127/ejm/10/3/0395>
- Holland, T. J. B., & Powell, R. (1998). An internally consistent thermodynamic data set for phases of petrological interest. *Journal of Metamorphic Geology*, 16(3), 309–343. <https://doi.org/10.1111/j.1525-1314.1998.00140.x>
- Holland, T. J. B., & Powell, R. (2003). Activity-compositions relations for phases in petrological calculations: An asymmetric multicomponent formulation. *Contributions to Mineralogy and Petrology*, 145(4), 492–501. <https://doi.org/10.1007/s00410-003-0464-z>
- Holland, T. J. B., & Powell, R. (2011). An improved and extended internally consistent thermodynamic dataset for phases of petrological interest, involving a new equation of state for solids. *Journal of Metamorphic Geology*, 29(3), 333–383. <https://doi.org/10.1111/j.1525-1314.2010.00923.x>
- Indares, A., White, R. W., & Powell, R. (2008). Phase equilibria modelling of kyanite-bearing anatectic paragneisses from the central Grenville Province. *Journal of Metamorphic Geology*, 26(8), 815–836. <https://doi.org/10.1111/j.1525-1314.2008.00788.x>
- Kohn, M. J., & Spear, F. (2000). Retrograde net transfer reaction insurance for pressure-temperature estimates. *Geology*, 28(12), 1127–1130. [10.1130/0091-7613\(2000\)028<1127:RNTRIF>2.3.CO;2](https://doi.org/10.1130/0091-7613(2000)028<1127:RNTRIF>2.3.CO;2)
- Konrad-Schmolke, M., O'Brien, P. J., de Capitani, C., & Carswell, D. A. (2008). Garnet growth at high- and ultra-high pressure conditions and the effect of element fractionation on mineral modes and composition. *Lithos*, 103(3–4), 309–332. <https://doi.org/10.1016/j.lithos.2007.10.007>
- Korzhinskii, D. S. (1959). *Physicochemical basis of the analysis of the paragenesis of minerals* (vol. 32, pp. 1–142). Consultants Bureau.
- Lanari, P., & Duisterhoef, E. (2019). Modeling metamorphic rocks using equilibrium thermodynamics and internally consistent databases: Past achievements, problems and perspectives. *Journal of Petrology*, 60, 19–56. <https://doi.org/10.1093/ptrology/egy105>
- Lanari, P., & Engi, M. (2017). Local bulk composition effects on metamorphic mineral assemblages. *Reviews in Mineralogy and Geochemistry*, 83(1), 55–102. <https://doi.org/10.2138/rmg.2017.83.3>
- Lanari, P., Giuntoli, F., Loury, C., Burn, M., & Engi, M. (2017). An inverse modeling approach to obtain P-T conditions of metamorphic stages involving garnet growth and resorption. *European Journal of Mineralogy*, 29(2), 181–199. <https://doi.org/10.1127/ejm/2017/0029-2597>
- Lanari, P., Guillot, S., Schwartz, S., Vidal, O., Tricart, P., Riel, N., & Beyssac, O. (2012). Diachronous evolution of the alpine continental subduction wedge: Evidence from P-T estimates in the Briançonnais Zone houillère (France - Western Alps). *Journal of Geodynamics*, 56–57, 39–54. <https://doi.org/10.1016/j.jog.2011.09.006>
- Lanari, P., & Piccoli, F. (2020). New horizons in quantitative compositional mapping – Analytical conditions and data reduction using XMAPTOOLS. *IOP Conference Series: Materials Science and Engineering*, 891, 012016. <https://doi.org/10.1088/1757-899X/891/1/012016>
- Lanari, P., Riel, N., Guillot, S., Vidal, O., Schwartz, S., Pêcher, A., & Hattori, K. H. (2013). Deciphering high-pressure metamorphism in collisional context using microprobe mapping methods: Application to the Stak eclogitic massif (northwest Himalaya). *Geology*, 41(2), 111–114. <https://doi.org/10.1130/G33523.1>
- Lanari, P., Vho, A., Bovay, T., Airaghi, L., & Centrella, S. (2019). Quantitative compositional mapping of mineral phases by electron probe micro-analyser. *Geological Society Special Publication*, 478(1), 39–63. <https://doi.org/10.1144/SP478.4>
- Lanari, P., Vidal, O., De Andrade, V., Dubacq, B., Lewin, E., Grosch, E. G., & Schwartz, S. (2014). XMapTools: A MATLAB®-based program for electron microprobe X-ray image processing and geothermobarometry. *Computers and Geosciences*, 62, 227–240. <https://doi.org/10.1016/j.cageo.2013.08.010>
- Loomis, T. P. (1979). A natural example of metastable reactions involving garnet and sillimanite. *Journal of Petrology*, 20(2), 271–292. <https://doi.org/10.1093/ptrology/20.2.271>
- Marmo, B. A., Clarke, G. L., & Powell, R. (2002). Fractionation of bulk rock composition due to porphyroblast growth: Effects on eclogite facies mineral equilibria, Pam Peninsula, New Caledonia. *Journal of Metamorphic Geology*, 20(1), 151–165. <https://doi.org/10.1046/j.0263-4929.2001.00346.x>
- Palin, R. M., Weller, O. M., Waters, D. J., & Dyck, B. (2016). Quantifying geological uncertainty in metamorphic phase equilibria modelling: A Monte Carlo assessment and implications for tectonic interpretations. *Geoscience Frontiers*, 7(4), 591–607. <https://doi.org/10.1016/j.gsf.2015.08.005>
- Powell, R. (1978). *Equilibrium thermodynamics in petrology: An introduction*. Harper & Row.
- Powell, R., & Holland, T. J. B. (1988). An internally consistent dataset with uncertainties and correlations: 3. Applications to geobarometry, worked examples and a computer program. *Journal of Metamorphic Geology*, 6(2), 173–204. <https://doi.org/10.1111/j.1525-1314.1988.tb00415.x>

- Powell, R., & Holland, T. (1994). Optimal geothermometry and geobarometry. *American Mineralogist*, 79(1–2), 120–133.
- Powell, R., & Holland, T. J. B. (2008). On thermobarometry. *Journal of Metamorphic Geology*, 26(2), 155–179. <https://doi.org/10.1111/j.1525-1314.2007.00756.x>
- Rubatto, D., Hermann, J., Berger, A., & Engi, M. (2009). Protracted fluid-induced melting during Barrovian metamorphism in the Central Alps. *Contributions to Mineralogy and Petrology*, 158(6), 703–722. <https://doi.org/10.1007/s00410-009-0406-5>
- Santamaría-López, Á., Lanari, P., & Sanz de Galdeano, C. (2019). Deciphering the tectono-metamorphic evolution of the Nevado-Filábride complex (Betic Cordillera, Spain) – A petrochronological study. *Tectonophysics*, 767. <https://doi.org/10.1016/j.tecto.2019.06.028>
- Scheffer, C., Vanderhaeghe, O., Lanari, P., Tarantola, A., Ponthus, L., Photiades, A., & France, L. (2016). Syn- to post-orogenic exhumation of metamorphic nappes: Structure and thermobarometry of the western Attic-Cycladic metamorphic complex (Lavrion, Greece). *Journal of Geodynamics*, 96, 174–193. <https://doi.org/10.1016/j.jog.2015.08.005>
- Spear, F. S. (1988a). Metamorphic fractional crystallization and internal metasomatism by diffusional homogenization of zoned garnets. *Contributions to Mineralogy and Petrology*, 99(4), 507–517. <https://doi.org/10.1007/BF00371941>
- Spear, F. S. (1988b). The Gibbs method and Duhem's theorem: The quantitative relationships among P, T, chemical potential, phase composition and reaction progress in igneous and metamorphic systems. *Contributions to Mineralogy and Petrology*, 99(2), 249–256. <https://doi.org/10.1007/BF00371465>
- Spear, F. S., & Pattison, D. R. M. (2017). The implications of overstepping for metamorphic assemblage diagrams (MADs). *Chemical Geology*, 457(Suppl C), 38–46. <https://doi.org/10.1016/j.chemgeo.2017.03.011>
- Spear, F. S., Thomas, J. B., & Hallett, B. W. (2014). Overstepping the garnet isograd: A comparison of QuiG barometry and thermodynamic modeling. *Contributions to Mineralogy and Petrology*, 168(3), 1–15. <https://doi.org/10.1007/s00410-014-1059-6>
- Steck, A., Della Torre, F., Keller, F., Pfeifer, H. R., Hunziker, J., & Masson, H. (2013). Tectonics of the leontine Alps: Ductile thrusting and folding in the deepest tectonic levels of the Central Alps. *Swiss Journal of Geosciences*, 106(3), 427–450. <https://doi.org/10.1007/s00015-013-0135-7>
- Tajčmanová, L., Connolly, J. A. D., & Cesare, B. (2009). A thermodynamic model for titanium and ferric iron solution in biotite. *Journal of Metamorphic Geology*, 27(2), 153–165. <https://doi.org/10.1111/j.1525-1314.2009.00812.x>
- Thompson, J. B. (1955). The thermodynamic basis for the mineral facies concept. *American Journal of Science*, 253(2), 65–103. <https://doi.org/10.2475/ajs.253.2.65>
- Todd, C. S., & Engi, M. (1997). Metamorphic field gradients in the Central Alps. *Journal of Metamorphic Geology*, 15(4), 513–530. <https://doi.org/10.1111/j.1525-1314.1997.00038.x>
- Trommsdorff, V. (1966). Progressive Metamorphose kieseliger Karbonatgesteine in den Zentralalpen zwischen bernina und Simplon. *Schweizerische Mineralogische Und Petrographische Mitteilungen*, 46, 431–460.
- Vidal, O., De Andrade, V., Lewin, E., Munoz, M., Parra, T., & Pascarelli, S. (2006). P-T-deformation-Fe³⁺/Fe²⁺ mapping at the thin section scale and comparison with XANES mapping: Application to a garnet-bearing metapelite from the Sambagawa metamorphic belt (Japan). *Journal of Metamorphic Geology*, 24(7), 669–683. <https://doi.org/10.1111/j.1525-1314.2006.00661.x>
- Vidal, O., & Parra, T. (2000). Exhumation paths of high-pressure metapelites obtained from local equilibria for chlorite-phengite assemblages. *Geological Journal*, 35(3–4), 139–161. <https://doi.org/10.1002/gj.856>
- White, R. W., Powell, R., & Baldwin, J. A. (2008). Calculated phase equilibria involving chemical potentials to investigate the textural evolution of metamorphic rocks. *Journal of Metamorphic Geology*, 26(2), 181–198. <https://doi.org/10.1111/j.1525-1314.2008.00764.x>
- White, R. W., Powell, R., & Holland, T. J. B. (2007). Progress relating to calculation of partial melting equilibria for metapelites. *Journal of Metamorphic Geology*, 25(5), 511–527. <https://doi.org/10.1111/j.1525-1314.2007.00711.x>
- White, R. W., Powell, R., Holland, T. J. B., Johnson, T. E., & Green, E. C. R. (2014). New mineral activity-composition relations for thermodynamic calculations in metapelitic systems. *Journal of Metamorphic Geology*, 32(3), 261–286. <https://doi.org/10.1111/jmg.12071>
- Whitney, D. L., & Evans, B. W. (2010). Abbreviations for names of rock-forming minerals. *American Mineralogist*, 95(1), 185–187. <https://doi.org/10.2138/am.2010.3371>
- Yakymchuk, C. (2017). Applying phase equilibria modelling to metamorphic and geological processes: Recent developments and future potential. *Geoscience Canada*, 44(1), 27–46. <https://doi.org/10.12789/geocanj.2017.44.114>
- Yakymchuk, C., Clark, C., & White, R. W. (2017). Phase relations, reaction sequences and petrochronology. *Reviews in Mineralogy and Geochemistry*, 83(1), 13–53. <https://doi.org/10.2138/rmg.2017.83.2>

SUPPORTING INFORMATION

Additional supporting information may be found online in the Supporting Information section.

Material S1 Analytical conditions for compositional mapping by EPMA

Material S2 Representative mineral compositions of garnet, plagioclase, muscovite and biotite

Material S3 Compositional maps for area 3

Material S4 T-in-biotite.

How to cite this article: Lanari P, Hermann J.

Iterative thermodynamic modelling—Part 2: Tracing equilibrium relationships between minerals in metamorphic rocks. *J Metamorph Geol*. 2021;39:651–674. <https://doi.org/10.1111/jmg.12575>

APPENDIX 1.

The model-quality factors for each simulation discussed in the text are presented below. Modelled mineral compositions are given in Table 3.

LBC1.1

P–*T* conditions 593°C, 0.65 GPa

Model evaluation $Q_{asm} = 100\%$
 $Q_{vol} = 95.48\%$
 $Q_{cmp} = 88.75\%$
 $Q_{total1} = 94.74\%$

$Q_{cmp}^{Pl2} = 99.83\%$ ($Q_{cmp}^{Pl1} = 89.67\%$)
 $Q_{cmp}^{Ms} = 72.23\%$
 $Q_{cmp}^{Bt} = 85.61\%$

Comments Optimal *P*–*T* conditions for the assemblage
 Pl_2+Bt
 Excluded phases: Ap

P–*T* conditions 620°C, 0.96 GPa

Model evaluation $Q_{asm} = 83\%$
 $Q_{vol} = 93.17\%$
 $Q_{cmp} = 90,895\%$
 $Q_{total1} = 78.91\%$

$Q_{cmp}^{Pl2} = 100\%$ ($Q_{cmp}^{Pl1} = 88.41\%$)
 $Q_{cmp}^{Ms} = 82.12\%$
 $Q_{cmp}^{Bt} = 79.75\%$

Comments T_{max} conditions
 Paragonite (1.4 vol.%) predicted to be
 stable, not observed
 Excluded phases: Ap

LBC2.1

P–*T* conditions 664°C, 0.94 GPa

Model evaluation $Q_{asm} = 100\%$
 $Q_{vol} = 95.43\%$
 $Q_{cmp} = 83.16\%$
 $Q_{total1} = 92.86\%$

$Q_{cmp}^{Pl2} = 82.43\%$
 $(Q_{cmp}^{Pl1} = 65.29\%)$
 $Q_{cmp}^{Ms} = 81.95\%$
 $Q_{cmp}^{Bt} = 75.51\%$
 $Q_{cmp}^{Grt} = 48.90\%$

APPENDIX 1. (Continued)**LBC2.1**

Comments Optimal *P*–*T* conditions for the
 assemblage $Ky+Pl_2\pm Bt$
 Excluded phases: Ap

P–*T* conditions 620°C, 0.96 GPa

Model evaluation $Q_{asm} = 75\%$
 $Q_{vol} = 74.96\%$
 $Q_{cmp} = 81.86\%$
 $Q_{total1} = 64.20\%$
 $Q_{cmp}^{Pl2} = 53.26\%$
 $(Q_{cmp}^{Pl1} = 45.44\%)$
 $Q_{cmp}^{Ms} = 82.68\%$
 $Q_{cmp}^{Bt} = 82.57\%$
 $Q_{cmp}^{Grt} = 39.67\%$

Comments T_{max} conditions
 Excluded phases: Ap

LBC2.2

P–*T* conditions 597°C, 0.67 GPa

Model evaluation $Q_{asm} = 100\%$
 $Q_{vol} = 93.22\%$
 $Q_{cmp} = 63.54\%$
 $Q_{tot} = 85.59\%$

$Q_{cmp}^{Pl2} = 36.53\%$
 $Q_{cmp}^{St} = 100\%$
 $Q_{cmp}^{Bt} = 59.64\%$
 $Q_{cmp}^{Grt} = 52.51\%$
 $Q_{cmp}^{Chl} = 75.28\%$

Comments Optimal *P*–*T* conditions for
 the assemblage
 $Grt+Bt+Chl+Pl+St$
 Excluded phases: $Ky+Ms+Ap+Rt$

(Continues)